To appear in the special issue on Mineral Dust in the Journal of Geophysical Research – Atmospheres 2001

Interactive soil dust aerosol model in the GISS GCM
1. Sensitivity of the soil dust cycle to radiative properties of soil dust aerosols

Jan Perlwitz[1]
Department of Applied Physics and Applied Mathematics, Columbia University, New York

Ina Tegen
Max Planck Institute for Biogeochemistry, Jena, Germany

Ron L. Miller
NASA Goddard Institute for Space Studies, New York

Abstract

The sensitivity of the soil dust aerosol cycle to radiative forcing by the soil dust aerosol particles themselves is studied. Four experiments with the NASA GISS atmospheric general circulation model, which includes a soil dust aerosol model, are compared, all using a prescribed climatological sea surface temperature as a lower boundary condition. In one experiment, dust is included as a dynamic tracer with no radiative effect, whereas dust interacts with radiation in the other simulations. The single-scattering albedo of dust particles is prescribed to be globally uniform in the experiments with radiatively active dust, although this albedo is varied from experiment to experiment. On a global scale the radiative forcing by dust generally causes a reduction in the atmospheric dust load, corresponding to a decreased dust source flux. The dust source flux and its changes are analyzed in more detail for the main source regions. This analysis shows that the reduction varies both with the season and with the single-scattering albedo of the dust particles. The experiments show that dust radiative forcing can lead to significant changes both in the soil dust cycle and in the climate state. To estimate dust concentration and radiative forcing by dust more accurately, dust size distributions and dust single-scattering albedo in the model should be a function of the source region, because dust concentration and the climate response to dust radiative forcing are sensitive to dust radiative parameters.

1. Introduction

The effect of tropospheric aerosols on the global climate via direct or indirect radiative forcing is one of the largest uncertainties in climate change studies [*Shine and de F. Forster*, 1999]. Among these aerosols, soil dust is an important climate forcing factor due to its high atmospheric load and optical thickness: 30% of the total aerosol optical thickness is attributed to soil dust aerosols, of which roughly half is estimated to be anthropogenic in origin [*Tegen and Fung*, 1995; *Tegen et al.*, 1996]. Although the highest dust concentrations are found over land, observations by direct measurements [*Prospero*, 1996], satellite retrievals [*Moulin et al.*, 1997; *Herman et al.*, 1997; *Husar et al.*, 1997], and model experiments [*Tegen and Fung*, 1994, 1995] reveal that a dust plume can extend thousands of kilometers offshore in certain regions. Dust aerosols dominate the light scattering downwind of dust source regions [*Tegen and Lacis*, 1996; *Li et al.*, 1996]. For example, *Alpert et al.* [1998] estimate that the 30 dusty days per year correspond to a heating rate of about 6 K per year in the lower atmosphere over the eastern tropical North Atlantic Ocean. In addition to its radiative effect, soil dust may also impact atmospheric chemistry by providing surfaces for heterogeneous chemical reactions [*Dentener et al.*, 1996; *Tabazadeh et al.*, 1998].

The soil dust cycle has been studied using off-line transport models to test source and sink parameterizations of soil dust [e.g. *Tegen and Fung*, 1995; *Marticorena and Bergametti*, 1996; *Schulz et al.*, 1998]. Other studies include dust as a tracer in a general circulation model (GCM) [*Joussaume*, 1990; *Genthon*, 1992; *Tegen and Miller*, 1998], the former two mainly simulate dust distributions under paleoclimate conditions. However, these studies did not include the radiative effect of dust on climate dynamics. The climate response to dust forcing has been addressed in only a few studies so far [*Coakley and Cess*, 1985; *Miller and Tegen*, 1998]. These studies used prescribed dust distributions that could not be modified by changes in the soil dust cycle caused by changes in the model dynamics forced by dust radiative heating. Other studies emphasized the great uncertainty of dust radiative forcing and its sensitivity to radiative parameters such as the dust single-scattering albedo [*Liao and Seinfeld*, 1998; *Claquin et al.*, 1998; *Sokolik and Toon*, 1999; *Miller and Tegen*, 1999].

In this paper we present new results of our work to assess the climate impact of soil dust aerosols using the National Aeronautics and Space Administration Goddard Institute for Space Studies (NASA GISS) atmospheric GCM (AGCM). There are two predecessor studies [*Tegen and Miller*, 1998; *Miller and Tegen*, 1998] which are continued here. In the work of *Tegen and Miller* [1998], soil dust was included as a dynamic tracer, but the radiative effect of dust upon the model climate and its feedback upon the dust distribution were not taken into consideration. In the *Miller and Tegen* [1998] work the radiative effect upon the model climate was examined using a prescribed soil dust aerosol distribution. In the current study, both approaches are combined. In the GISS AGCM, soil dust is included as a dynamic tracer whose distribution is a function of various climate variables. Radiative forcing by dust changes the climate variables in the model such as the surface wind and rainfall, which in turn influence dust emission, transport, and deposition; that is, the soil dust aerosol model is fully coupled with the other climate variables in the AGCM.

Dust optical properties should vary with the mineralogical composition of the source region. However, for simplicity, and to minimize the computational burden, we assign the optical properties of all source regions using measurements of far-traveled Saharan dust according to *Tegen and Lacis* [1996]. Because the top of atmosphere (TOA) radiative forcing of Saharan dust is coincidentally poised between heating and cooling of the column [*Miller and Tegen*, 1999], our choice may underestimate the effect of dust on climate. Thus we carried out sensitivity experiments with varying radiative properties of the dust particles, represented by the single-scattering albedo ϖ of dust. The sensitivity of our results to the single-scattering albedo will indicate the importance of parameterizing the optical properties of each dust source region separately. In this paper the analysis emphasizes the modifications of the soil dust aerosol cycle due to radiative forcing by dust, as well as its sensitivity to the radiative properties of the dust particles. The climate impact of interactive dust will be inspected in a companion study, although the global averaged effect of dust upon climate is briefly discussed in section 7.

2. Model and Experiments

The soil dust aerosol model embedded in the GISS AGCM [*Hansen et al.*, 1997] is described in detail by *Tegen and Miller* [1998]. The AGCM has a horizontal resolution of 4° latitude by 5° longitude and 12 vertical layers. Documentation of the convection and cloud parameters is given by *Del Genio et al.* [1996]. The ground hydrology parameterization and planetary

boundary layer treatment are described by *Rosenzweig and Abramopoulos* [1997] and *Hartke and Rind* [1997], respectively. The planetary boundary layer (PBL) treatment parameterizes drag and mixing coefficients based on similarity theory. Transfer coefficients are determined separately for heat, momentum, and moisture. The model surface layer is defined to be an equal flux layer. Surface fluxes are calculated using a wind profile model which extrapolates the wind downward from the first model layer. Compared to a former version of the GISS AGCM [*Hansen et al.*, 1983], the new convection and PBL parameterizations led to improved atmospheric circulation [*Druyan et al.*, 1995], interhemispheric transport of tracers [*Rind and Lerner*, 1996], vertical profile of heating [*Del Genio and Yao*, 1993], and geographical distribution of low-latitude precipitation [*Druyan et al.*, 1995]. The physically based ground hydrology parameterization has six soil layers with realistic hydraulic conductivity and matric potential functions. A vertical profile of soil textures is defined according to assigned soil type. The scheme explicitly includes processes of transpiration, evaporation from precipitation or dew intercepted by the vegetation canopy, evaporation from bare soils, infiltration, and runoff. Underground runoff is a sink for some of the groundwater.

The parameterization of dust as a tracer follows the calculation of dust in the off-line GISS tracer transport model [*Tegen and Fung*, 1994]. In this model the soil dust particles are partitioned into four size classes (< 1, 1-2, 2-4, and 4-8 μm), which are carried as separate tracers. Particles smaller than 1 μm are transported as one class because they are not strongly fractionated by gravitational settling. Particles larger than 8 μm are responsible for only about 1% of the dust radiative forcing [*Tegen et al.*, 1996]. The surface distributions of clay (particles smaller than 1 μm) and small silt (particle radius between 1 μm and 10 μm) were derived from a global soil texture data set [*Zobler*, 1986; *Webb et al.*, 1991].

Dust deflation is parameterized according to *Gillette* [1978]. It is proportional to the cube of the surface wind speed, with the constraint that the speed must exceed a threshold velocity,

$$q_a = C(u - u_{tr})u^2, \tag{1}$$

where q_a is the dust flux from the surface in $\mu\mathrm{g\,m^{-2}\,s^{-1}}$, u is the surface wind speed in $\mathrm{m\,s^{-1}}$, and u_{tr} is the threshold velocity. C is a dimensional constant, which amounts to $2\,\mu\mathrm{g\,s^{-2}\,m^{-5}}$ and $5\,\mu\mathrm{g\,s^{-2}\,m^{-5}}$ for clay and silt, respectively. The threshold velocity varies between 4 and $10\,\mathrm{m\,s^{-1}}$ depending on the location. The variations are designed partly to account for sub-grid-scale wind variability [*Tegen and Miller*, 1998]; that is, the threshold velocity is lower in grid boxes with high sub-grid-scale variations in wind, as estimated by the 1° latitude by 1.25° longitude European Centre for Medium-Range Weather Forecasts (ECMWF) analyses of surface wind. In addition, dust emission only can occur when the soil moisture is low. To fulfill this condition in the model, evaporation in a grid box must exceed precipitation for a certain time period which depends on the soil texture. In addition, dust deflation is only allowed in desert or sparsely vegetated areas labeled by *Matthews* [1983], as well as from disturbed soils that are affected by deforestation, cultivation in dry regions, wind erosion, and the shift in the Saharan/Sahelian boundary [*Middleton and Thomas*, 1992; *World Resources Institute (WRI)*, 1992; *Tucker et al.*, 1991].

Following deflation, dust is advected by the model winds. Dust is also subject to sub-grid-scale vertical mixing by the convection parameterization. Dust removal takes place by gravitational settling, turbulent mixing in the first model layer, and subcloud washout, which is calculated using AGCM precipitation. The efficiency of the dust removal by rain is described using the scavenging ratio Z, the ratio of the mass of dust per mass unit of rainwater C_{rain} in $\mathrm{g\,kg^{-1}}$ to the mass of dust per mass unit of air C_{air} in $\mathrm{g\,kg^{-1}}$,

$$Z = C_{rain}/C_{air}. \tag{2}$$

Here a scavenging ratio of 700 is used according to *Tegen and Fung* [1994].

Dust radiative forcing is calculated with the GISS AGCM radiation model, which is based upon the k distribution and doubling-adding methods. Radiative parameters for the different particle sizes are determined via Mie calculations using refractive indices for far-traveled Saharan dust from *Volz* [1973] and *Patterson and Gillette* [1977]. For the calculation of dust radiative effect, the submicron size class is further subdivided into four size classes according to *Tegen and Lacis* [1996]. According to Mie theory, dust particles are approximated as perfect spheres. This causes a misestimation of the scattering phase function for dust particles. Although this is important for remote sensing application, the idealization has little effect upon the radiative flux divergence that represents the climate forcing [*Lacis and Mishchenko*, 1995].

Four experiments were carried out using both a prescribed climatological sea surface temperature (SST)

and a sea ice distribution as a lower boundary condition. In one of the four experiments, dust is a dynamic tracer without any radiative effect. Hereinafter we refer to this experiment as the "passive dust" experiment. In the remaining three experiments, radiative forcing by dust is taken into consideration. The single-scattering albedo of far-traveled Saharan dust particles (ϖ_0) is prescribed for dust from all source regions in the first of these three experiments. This albedo depends on the dust particle size and wavelength ($1\,\mu$m size: $\varpi_0 = 0.86$; $0.5\,\mu$m size: $\varpi_0 = 0.92$ at $0.55\,\mu$m wavelength) [*Tegen and Lacis*, 1996]. Hereinafter we refer to this experiment as the "baseline experiment." In the remaining two experiments, the single-scattering albedo is decreased or increased for all source regions and wavelengths by 10%, representing more absorbing ($0.9\varpi_0$) or reflecting dust ($1.1\varpi_0$), respectively, to evaluate the sensitivity of the dust cycle to changing radiative properties of the dust particles. For the more reflecting case, ϖ is set equal to unity at wavelengths where the 10% increase would otherwise exceed this value. The first year of model output was discarded to eliminate trends associated with spin-up, after which 26 years were simulated in each experiment.

3. Sensitivity of Soil Dust Emission

3.1. Some Remarks About the Approach

Dust emission is favored by high surface winds and evaporation exceeding precipitation over an extended period of time. Changes in the wind speed, related to changes in the dust emission, can occur over various space and timescales. These can be local phenomena which affect the variability at short timescales, or changes in the large-scale quasi-stationary patterns of the circulation.

To identify the processes that change dust emission in the main source regions, we calculated the local correlation coefficients between the time series of the monthly averaged dust source flux and the time series of other variables. These variables are the monthly averaged number of wind events above the threshold velocity for dust emission (n_{tr}), the monthly averaged wind speed (v), the magnitude of the monthly averaged horizontal wind vector ($\|\vec{\mathrm{v}}\|$), and the monthly averaged difference of precipitation and evaporation. We expect the highest correlations between the dust source flux and the n_{tr}. The correlation of the flux with v includes fluctuations at short and long timescales, since it is calculated from the horizontal wind vector at each time step. By calculating the magnitude of the monthly averaged wind vector $\|\vec{\mathrm{v}}\|$, changes in wind speed on a short timescale are averaged out. Hence changes in $\|\vec{\mathrm{v}}\|$ can be interpreted as changes in the circulation on a monthly or longer timescale. We hypothize less correlation between this variable and the dust source flux, compared to the correlation between the latter and either n_{tr} or v. In this section we diagnose the changes in the patterns of dust emission obtained in our experiments. We are interested in the seasonal dependence of the changes. Thus differences are shown for the seasonal average (December/January/February (DJF); March/April/May (MAM); June/July/August (JJA); September/October/November (SON); annual average (ANN)). However, calculating a correlation between the seasonal averages of two variables can lead to misinterpretation, because anomalies in time from the seasonal average can be caused by anomalies in different months of a season. Those would lead to a faulty positive (or negative) correlation coefficient. Therefore the correlations were calculated using the monthly averages of the variables to reduce such source of error. They were calculated for the variables from the passive dust experiment, and for the anomalies in the experiments with radiatively active dust with respect to the long-term means from the passive dust experiment. We are mainly interested in the correlation between the changes of the variables when the experiments with radiatively active dust are compared to the passive dust experiment. Therefore the annual cycle was not removed prior to calculating the correlations.

Although the difference of precipitation and evaporation is a constraint upon the dust source flux, we did not find any significant correlation between changes in these two variables.

3.2. Global Dust Emission

In the AGCM experiment in which dust is a dynamic tracer with no radiative effect, the globally averaged dust emission is $1312 \pm 97\,\mathrm{Mt\,yr^{-1}}$ (mean plus or minus one standard deviation based on yearly means). This amount is about 40% larger than the emission obtained from a similar experiment carried out in a former study with the nine layer GISS GCM [*Tegen and Miller*, 1998, experiment A]. The difference is caused by higher wind speeds at the surface using the 12 layer version of the model for the current study. However, both global totals are somewhat arbitrary: the proportionality coefficient C in equation (1) has been chosen so that the global total in the nine layer model is consistent with global estimates based on observations [*Tegen and Fung*, 1994]; that is, C could be recalibrated to bring

the 12 layer model total in line with the nine layer value. Rather than recalibrate, we simply note that each value is within the range of other estimates which are widely separated [see *Duce*, 1995].

A comparison of the total dust emission in the various experiments is given in Table 1. The time mean and the interannual standard deviation are presented both for the entire year and for the individual seasons. In the experiment with radiatively inactive dust, the passive dust experiment, the emission shows a maximum in Northern Hemisphere (NH) spring and summer, and a minimum in autumn. In the experiments, including the radiative effect of dust, the yearly emitted amount of dust is about 15 to 20% lower than in the passive dust experiment. In the course of the year the reduction varies both with the season and with the prescribed single-scattering albedo. In winter the largest decrease is found for more absorbing dust, whereas in summer, the largest decrease is found for more reflecting dust. There is also a tendency of decreased interannual variability in the experiments which include the radiative effect of dust.

3.3. Sahara/Sahel Source Region

The largest contribution to globally emitted dust is from the Sahara/Sahel source region (Table 2). This region emits $592 \pm 55\,\mathrm{Mt\,yr^{-1}}$ of dust in the passive dust experiment. This value is reduced by 12 to 15% in all experiments, which include the radiative effect of dust. The season during which this reduction is largest depends on the particle single-scattering albedo. During DJF, dust emission is most reduced for more absorbing dust, whereas for JJA, dust emission is most reduced for more reflecting dust.

Plate 1 displays the horizontal distribution of the seasonally averaged dust source flux (shown as numbers in $\mathrm{mg\,m^{-2}\,d^{-1}}$) and surface wind vector (arrows) in the Sahara/Sahel region in NH winter of the passive dust experiment, along with changes in the experiments with radiatively active dust. In addition, correlations (shades) between source flux and $\|\vec{v}\|$ are shown. All correlation coefficients represented by shaded grid boxes in the plates of this source region and the figures of the other source regions are statistically significant (t-test) at a confidence level of 95% or greater. In addition, correlation coefficients are only presented for grid boxes where the anomalies in both variables are statistically distinct from zero at a confidence level of 50% or greater. This lower confidence level was chosen to emphasize the spatial patterns of the anomalies. However, the largest anomalies in the wind variables and the dust emission are also statistically significant at a confidence level of 95% or greater.

In the passive dust experiment during NH winter, the Sahel region along with the western and northeastern Sahara contribute most to the total dust emission in North Africa. The emission is positively correlated with $\|\vec{v}\|$, which is related to the trade winds in this region, in particular in western Sahara and the Sahel region.

For more absorbing dust, the strong decrease in dust emission relative to the passive dust experiment is found mainly in the eastern part of the Sahara/Sahel source region, whereas there is actually an increase in emission in northwestern Sahara. Some positive correlation between the change in the dust source flux and the change in the quasi-stationary circulation is found both in northwestern Africa and in the eastern Sahel. The visual examination of the difference vector of the seasonally averaged surface wind indicates an increase and decrease, respectively, in the trade winds in these both regions. In the other two experiments with radiatively active dust, the winter changes in the dust source flux are generally smaller. The grid boxes in western Africa where the source flux increases have only a minor contribution to the total source flux in North Africa.

During NH summer in the passive dust experiment (Plate 2), the largest contribution to the dust emission in North Africa originates from the northeastern and eastern part. In this region the dust source flux is positively correlated with the large-scale circulation, in particular with the Indian monsoon flow over eastern Africa.

In the experiments with radiatively active dust, dust emission in the Sahara/Sahel source region is most reduced in the experiment with more reflecting dust (see Table 2), because of a significant decrease in the emission in northeastern Africa. In several grid boxes, where an evident change in the dust source flux is found, those changes are positively correlated with changes in $\|\vec{v}\|$. The visual examination of the stationary wind vector reveals that these changes are linked to changes in the Indian monsoon circulation. For more absorbing dust, the monsoon-induced flow is strongly enhanced, whereas for more reflecting dust, the Indian monsoon is weakened. In both cases this leads to a specific pattern of changes in the dust emission. In the baseline experiment, a slightly strengthened monsoon is found. Especially for more reflecting dust, the decrease in the Indian monsoon causes the strong decrease in the emitted dust integrated over the whole region. However, the correlations between changes in the monthly averaged dust emission and changes in v, which were also calculated (but

not shown), are higher and statistically significant in more grid boxes than the correlations between changes in the source flux and changes in $\|\vec{v}\|$, indicating that the changes in dust emission cannot only be explained by changes in the large-scale quasi-stationary circulation. Processes with short timescales also seem to have an important effect on the changes in the dust emission in North Africa.

3.4. Arabian Peninsula Source Region

The dust emission from the Arabian Peninsula has two peaks, one in winter and the other one in summer (Table 2). In the passive dust experiment, the total amount of the yearly emitted dust is $56.5 \pm 11.9\,\mathrm{Mt\,yr^{-1}}$. For more absorbing dust, this amount is about 10% higher, but for more reflecting dust about 20% lower, a difference that can be attributed mainly to the NH summer months. In the other seasons, there is a tendency of a reduced dust emission for all experiments with radiatively active dust.

The largest part of the dust amount emitted from the Arabian Peninsula in the passive dust experiment originates along the Yemeni coast (Plates 1 and 2). An additional amount comes from a grid box at the head of the Persian Gulf.

In the experiments with radiatively active dust, the main changes in the emission are found in NH summer (Plate 2). The emission increases both at the head of the Persian Gulf and the Yemeni coast for more absorbing dust and, with a smaller magnitude, in the baseline experiment, whereas it decreases at these grid boxes given more reflecting dust. These changes are positively correlated with changes in $\|\vec{v}\|$. They are related to an enhanced (diminished) Indian monsoon circulation for more absorbing (reflecting) dust.

3.5. Central Asia Source Region

Here central Asia is defined as the region around the Caspian Sea and the Aral Sea. Central Asia's dust emission in the passive dust experiment shows a strong annual cycle with a maximum of $35.7 \pm 13.5\,\mathrm{Mt\,month^{-1}}$ in NH summer and a minimum of only $1.8 \pm 1.2\,\mathrm{Mt\,month^{-1}}$ in winter (Table 2). The yearly emission amounts to $211 \pm 58\,\mathrm{Mt\,yr^{-1}}$, which is reduced in each experiment with radiatively active dust. This reduction increases with increasing single-scattering albedo from $36\,\mathrm{Mt\,yr^{-1}}$ for $0.9\varpi_0$ to $72\,\mathrm{Mt\,yr^{-1}}$ for $1.1\varpi_0$, largely as a result of differences during the NH summer months.

Figure 1 displays the horizontal distribution of the dust emission in the passive dust experiment during Northern Hemisphere summer, its changes in the experiments with radiatively active dust. In addition, the correlation with the surface wind speed is shown, instead of the correlation with $\|\vec{v}\|$, since there are only uncertain results from the correlation between dust emission and large-scale circulation. In the passive dust experiment, the main areas of dust emission are located north of the Caspian Sea and east of the Aral Sea. North of the Caspian Sea, dust emission is smaller in all experiments that include radiatively active dust. In contrast, the changes in the emission depend on the single-scattering albedo in the Aral Sea region. There, the emission increases for more absorbing dust, whereas they decrease for more reflecting dust. There is some positive correlation of these changes with changes in the surface wind speed, which increases (decreases) in this region, in particular southeast of the Aral Sea, for more absorbing (reflecting) dust. In many grid boxes, there is also a strong correlation of the changes in the dust source flux with changes in the number of wind events above the critical threshold velocity (not shown). Generally, these results indicate that the described changes in the dust emission are mainly due to changes both in mean wind speed and wind speed variability on shorter timescales.

3.6. East Asia Source Region

East Asia's dust source region emits $55.2 \pm 21.5\,\mathrm{Mt\,yr^{-1}}$ in the passive dust experiment (Table 2). The largest amount is contributed during NH spring. In this season a maximum of $13.1 \pm 5.8\,\mathrm{Mt\,month^{-1}}$ is found. In contrast, only little dust is emitted during winter and autumn. The inclusion of radiative forcing generally leads to a reduced dust emission. In all seasons, except in winter, dust emission decreases with increasing particle absorptivity. The relative decrease in dust emission is largest in summer. The annual emission is reduced by 35% and 13% for $0.9\varpi_0$, and $1.1\varpi_0$, respectively.

The horizontal distribution of dust emission in the east Asia source region and correlations are not shown because of a lack of significance of the correlation between the dust source flux and the other variables. In the passive dust experiment, the region that mainly contributes to the total dust emission is located between 105° and 120°E and 40° and 48°N. In particular during NH summer, when the relative reduction in the emission is largest, some grid boxes with a positive correlation between changes in the dust source flux and changes in the surface wind speed as well as in n_{tr} are found. We did not find any correlation with $\|\vec{v}\|$. This indicates that decreased dust emission in east Asia's source region is mainly caused by processes with small timescales and

not due to changes in the large-scale circulation. This dependence is similar to that in Central Asia.

3.7. North America Source Region

The dust emission in North America amounts to $114 \pm 42\,\mathrm{Mt\,yr^{-1}}$ in the passive dust experiment (Table 2). In NH spring, the maximum amount is emitted, corresponding to $14.7 \pm 7.1\,\mathrm{Mt\,month^{-1}}$. The emission in each of the other seasons is about half of this value. In all seasons, less dust is emitted in the experiments that include the radiatively active dust. The reduction of the annual total is between 12% and 33%.

Figure 2 displays the horizontal distribution of dust emission in the passive dust experiment during NH spring, its changes in the experiments with radiatively active dust, and its correlation with the surface wind speed. In the passive dust experiment, dust emission is largest over the Great Plains.

In the experiment with radiatively active dust, dust emission is reduced in the southern part. In this region, the reduction increases with increasing particle absorptivity (as in east Asia). These changes show some positive correlation with changes in the surface wind speed, in particular for more absorbing dust and in the baseline experiment. In addition, there is an even stronger correlation with the number of wind events. In the northern source region, there is also a tendency of reduced emission in all experiments with radiatively active dust but with no clear dependence on the particle single-scattering albedo. We did not find any correlation between changes in the dust emission and changes in $\|\vec{v}\|$. This indicates that the reduction in the dust emission is mainly due to processes with short timescales related to a decrease both in the wind speed and its variability.

3.8. Australia Source Region

Australia's dust emission amounts to $225 \pm 54\,\mathrm{Mt\,yr^{-1}}$ in the passive dust experiment (Table 2). Almost half the amount is contributed during Southern Hemisphere (SH) summer. The minimum in the annual cycle is found during SH winter. In the experiments with radiatively active dust, the yearly averaged emission is about 20% lower. In the various seasons, the decrease ranges from 11 to 27% without any clear dependence on either the particle single-scattering albedo or the season.

In Figure 3, the horizontal distribution of the dust source flux in the passive dust experiment, its changes in the experiments with radiatively active dust, and its correlation to the surface wind speed in Australia during SH summer are presented. In the passive dust experiment, dust is emitted over the whole central part of Australia with a maximum from a grid box located along the southern coast. The dust source flux is positively correlated with the surface wind speed where maximum emission is found.

A significant decrease in dust emission is found in all of the experiments that include the radiative effect of dust. The changes in the dust emission are positively correlated with changes in the surface wind speed. There is a more evident correlation of the change in the dust source flux with a change in the number of wind events above the critical threshold velocity (not shown). We did not find any correlation between the changes in the emission and changes in $\|\vec{v}\|$. Changes in emission seem to be caused mainly by changes in the mean wind speed and changes in the wind speed variability on a short timescale.

We caution that the results from our sensitivity experiments concerning the Australia source region are very uncertain. It will be shown in section 6 that the emissions in the model seem to be strongly overestimated, in particular during SH summer, compared to results from AVHRR satellite data.

In this section we have analyzed how the dust emission changes, if the radiative effect of dust is taken into consideration in the model. In summary, we have shown that this radiative effect leads to a reduced dust source flux into the atmosphere for the global average in all seasons and for almost all main dust source regions. In general, this indicates a negative feedback of dust radiative forcing upon dust emission. The amount of the reduction varies both with the season and with the single-scattering albedo of dust particles, depending on the region where dust deflation takes place. During winter in each hemisphere, in all regions with significant deflation, the reduction is larger for more absorbing than for more reflecting dust. During summer, this trend is generally reversed: the reduction in emission is larger for more reflecting dust, apart from east Asia and North America.

In the Sahara/Sahel source region and in the Arabian Peninsula we found a positive correlation, which is statistically significant, between changes in dust emission and changes in the magnitude of the monthly averaged surface wind vector which represents large-scale circulation patterns. In winter, changes in the dust source flux are related to changes in the trade winds, whereas in summer, they are related to changes in the Indian monsoon circulation.

The seasonal dependence of the global dust emission mainly reflects the seasonality of the North African and

Arabian source regions, the largest contributors to the global emission.

4. Dust Concentration in the Experiments

The global mean and standard deviation of dust concentration in the various experiments are presented in Table 3; the atmospheric dust load has features that are similar to those of the dust emission. In the passive dust experiment, the annual and global mean dust concentration averaged over all layers amounts to $3.71 \pm 0.25\,\mu g\,kg^{-1}$. The dust load has its maximum in NH spring and summer, and its minimum in autumn. In the experiments that include the radiative effect of dust, the yearly averaged dust concentration is reduced. The reduction ranges from 13 to 21%, varying according to season and prescribed single-scattering albedo. In winter, the largest decrease is found for more absorbing dust, whereas in summer, the largest decrease is found for more reflecting dust. There is also a tendency toward decreased variability in the experiments that include the radiative effect of dust.

The horizontal distribution of dust concentration in the passive dust experiment during NH winter and summer, and its changes in the experiments with radiatively active dust are presented in Figures 4 and 5, respectively. The changes relative to the passive dust experiment were tested for statistical significance using Student's t-test. Increases (decreases) at a confidence level of 95% or greater are shown by dark (light) shading in the pictures.

In the passive dust experiment in NH winter (Figure 4a), a dust cloud is located over North Africa extending over the tropical Atlantic. The maximum is located over the southern part of North Africa. Another major dust cloud is located over Australia, and a minor maximum of the dust concentration is found over North America.

The change in the dust concentration due to radiative effect of dust evidently varies over the various dust source regions depending on the season and the single-scattering albedo. In winter, the dust concentration shows its strongest reduction of 20-30% over the Sahara/Sahel source region in the experiment with more absorbing dust. In contrast, the dust concentration over this region is larger with increased single-scattering albedo. This corresponds to enhanced dust emission in this region. Another source region that is perturbed by dust radiative forcing during NH winter is located in Australia. There, dust emission and concentration are reduced by 20-30% for radiatively active dust for all three values of the particle single-scattering albedo of dust.

In summer (Figure 5), in contrast to winter, the strongest reduction of the dust concentration is found in the experiment with more reflecting dust over the Sahara/Sahel source region and, additionally, over the Arabian Peninsula and central Asia, which are also important source regions in this season. There, the dust load is about 50% lower in comparison to the passive dust experiment. In the experiment with more absorbing dust this reduction is much smaller. Over the Arabian Peninsula and northeastern Africa, even an increase in the dust load is found. In contrast, the dust concentration decreases more strongly for more absorbing dust than for more reflecting dust over North America and east Asia, although these are minor dust source regions in summer.

In NH spring and autumn the changes in dust concentration as a result of dust radiative forcing show a transition state between the winter and the summer change patterns. Despite the changes in the dust concentration, seasonal features, such as the spring maxima of the dust emission in North America and east Asia, are preserved in the experiments that include the radiative effect of dust.

In all seasons the dust concentration is higher (lower) in high and midlatitudes in low dust regions in the experiment with more absorbing (reflecting) dust. These changes are statistically significant because of a very small variability in the dust concentration in those regions. This response in the experiments with radiatively active dust could be caused by a longer (shorter) persistence of very small dust particles in the atmosphere due to a decreased (increased) deposition. Another possibility is an intensified (weakened) transport into the low dust regions.

We also compared the seasonal interannual variability by examining the standard deviation of the dust concentration in the experiments. The experiments including the radiative effect of dust do not differ significantly to another. However, there are some differences with respect to the passive dust experiment.

In Figure 6 the standard deviation of the dust concentration during NH winter and summer, respectively, is presented for the passive dust and the baseline experiment. The interannual variability of the dust concentration is high, with a standard deviation 20 to 50% of the mean. In winter, the maximum values of the standard deviation are evidently smaller over the main dust source regions for radiatively active dust. The decrease

amounts to about 30% and 50% over North Africa and Australia, respectively. In the areas with low dust concentration, the interannual variability is similar for all experiments.

In contrast, the maximum NH summer values of the standard deviation do not significantly decrease in the baseline experiment. Over the Aral Sea source region, even an evident increase, which amounts to about 40%, is found. A similar result was also obtained for more absorbing dust, whereas the interannual variability decreases in this region for more reflecting dust. In spring and autumn the dust response resembles the results for winter. Changes in the seasonal interannual variability seem to reflect features of the changes in the seasonal long-term averages. Where a decrease in the mean dust concentration is found, there is also a tendency to a decreased variability and vice versa.

5. Dust Deposition in the Experiments

The global mean wet deposition and dry turbulent deposition of dust and their standard deviations are shown in Tables 4 and 5, respectively, for the various seasons and the entire year. The annual long-term average and the global mean of wet deposition and dry turbulent deposition of dust amount to about 579 ± 42 and $193.8 \pm 14.4\,\mathrm{Mt\,yr^{-1}}$, respectively. Unfortunately, an error occurred when saving the deposition by gravitational settling, so we are not able to present this variable and the total deposition here. However, assuming that dust emission and deposition are in equilibrium in the long term, it can be estimated that gravitational settling accounts for almost the half of the totally deposited dust in our experiments. The sensitivity of the deposition in the various seasons to the changed radiative properties of the dust particles is consistent with the sensitivity found for the dust emission and dust concentration.

The horizontal patterns of dry turbulent deposition are very similar to the patterns of the dust concentration. Where the dust concentration is high, the dry turbulent deposition is high. Also, the anomaly patterns in the sensitivity experiments evidently match each other. Therefore the horizontal patterns of dry turbulent deposition are not shown here.

The horizontal pattern of wet deposition of dust in the passive dust experiment and its changes in the experiments with radiatively active dust are displayed in Plates 3 and 4 for NH winter and summer, respectively. Only changes in this variable which are statistically significant in the experiments with radiatively active dust relative to the passive dust experiment are shown. The confidence level is 95% or greater again, based on Student's t-test.

Wet deposition of dust is a function of both the dust concentration and the precipitation. In NH winter (Plate 3) a band of maximum washout is found in the Intertropical Convergence Zone (ITCZ) over Africa and the equatorial Atlantic. Large dust removal by rain also takes place over western Australia and offshore northwest of this continent. Comparing the various experiments with radiatively active dust, the wet deposition in the ITCZ over Africa and the equatorial Atlantic decreases the most for more absorbing dust. This result is consistent with the one from the dust emission and dust concentration. In addition, it shows that the decrease in the dust concentration in this region, which is also larger for more absorbing dust, is not caused by an increased dust removal.

In NH summer (Plate 4), in the passive dust experiment, large washout of dust by rain is found in regions with tropical precipitation in a band extending from the equatorial Atlantic over North Africa to the Indian subcontinent with a maximum over the Arabian Sea, which is about $150\,\mathrm{mg\,m^{-2}\,d^{-1}}$. Maxima of wet deposition are also related to midlatitude precipitation in the Northern Hemisphere, such as in eastern North America, northeastern Europa, and east Asia. In the experiments with radiatively active dust, the largest decrease of wet deposition of dust is found in the experiment with more reflecting dust over North Africa, the Arabian Peninsula, and India. This sensitivity to single-scattering albedo is consistent with that from dust emission and dust concentration. In the experiment with more absorbing dust, there is a large increase in the dust washout over the Arabian Peninsula and the Indian subcontinent, which amounts to about $100\,\mathrm{mg\,m^{-2}\,d^{-1}}$ in the maximum. The precipitation shows also a statistically significant increase in this region. There is a similar pattern in the baseline experiment but with much smaller magnitude. These changes can be attributed to the enhanced Indian monsoon circulation in both experiments, which also was seen in the wind vectors analyzed in section 3.

6. Comparison to AVHRR Satellite Data

6.1. Some Remarks About the Approach

To evaluate the model capability to reproduce the observed dust load in the atmosphere and its interannual variability, we compared the dust optical thicknesses from the experiments to satellite retrievals de-

rived from the National Oceanic and Atmospheric Administration (NOAA) advanced very high resolution radiometer (AVHRR) instrument [*Rao et al.*, 1988; *Stowe et al.*, 1997; *Husar et al.*, 1997]. These data are available for the years 1982 to 1992 and 1996/1997. Model dust extinction optical thicknesses are calculated according to *Tegen and Fung* [1994]. Such a comparison of modeled and satellite-derived optical thickness is not straightforward. In the AVHRR satellite retrievals, dust is assumed to be totally reflecting. Thus the retrievals provide a lower limit of the dust optical thickness in regions with high dust concentration, in particular for more absorbing dust. For more reflecting dust, we can expect a less ambiguous comparison between modeled and measured optical thickness. An additional problem occurs, in regions with low dust concentration, where other aerosol types can significantly contribute to the optical thicknesses of the retrievals. There, the modeled optical thicknesses are expected to be lower than the satellite retrievals.

Another source of comparison uncertainty is the different size distribution of aerosol particles assumed by the AVHRR satellite retrievals [*Stowe et al.*, 1997] and the model. In the model, dust aerosol size distributions are calculated dynamically and vary with each grid box, whereas fixed sizes are assumed for satellite retrievals. An additional complication is particle nonsphericity, which is not taken into consideration in the model. The comparison is also limited by the fact that the AVHRR retrievals only cover optical thicknesses over sea.

Despite these uncertainties a comparison of the model results to the retrievals is a useful approach to identify regions where the model results are inconsistent with the observations, even if only a coarse evaluation is possible. However, as a consequence of these uncertainties, we cannot distinguish which experiment best represents the observations.

6.2. Comparison of the Mean Optical Thickness

In Plate 5 the differences between the mean optical thickness from the baseline experiment and from the AVHRR satellite are presented for all seasons. In NH winter the simulated dust optical thickness offshore the western coast of North Africa between 20°N and 30°N is about 0.1 higher than in the observations. This difference increases with decreasing single-scattering albedo of dust. Other aerosols than soil dust do not significantly contribute to the total optical thickness in this region [*Tegen et al.*, 1997]. Therefore the observed optical thickness should in this region be a lower limit considering dust absorption. The dust load in this region is relatively insensitive to the particle single-scattering albedo in our experiments. Hence the optical thickness in the experiments is consistent with the observations. In contrast, in NH spring the optical thickness in this region is overestimated in the experiments compared to satellite data, although for radiatively active dust, the results are closer to observations than for radiatively inactive dust.

In NH winter and spring, over the equatorial Atlantic, carbonaceous aerosols significantly contribute to the total optical thickness [*Liousse et al.*, 1996; *Penner et al.*, 1998], so the observed optical thickness should be higher than the simulated one. Therefore the results of our experiments are not inconsistent with the observations.

In NH spring the lower optical thickness east of the Chinese coast in the experiments is consistent with the observations, because east Asia's deserts are not the only aerosol source during this season. In particular, sulfate and carbonaceous aerosols also significantly contribute to the observed optical thickness in this region [*Tegen et al.*, 1997; *Penner et al.*, 1998; *Tegen et al.*, 2000]. The Indian subcontinent and the eastern Mediterranean are located at the edge of the dust cloud. These regions are also influenced by industrial aerosols. Thus the lower optical thicknesses simulated in these regions are consistent with the observed ones.

In NH summer, in the areas with maximum dust concentration over the Arabian Sea and central Asia, the simulated optical thickness in the baseline experiment is higher by more than 0.4 compared to the observations, indicating an overestimation in the model, or an underestimation in the satellite retrievals. In contrast, further away from the center of the dust cloud, over both India and the eastern Atlantic around 10°N, the dust optical thickness in the experiments is lower by more than 0.2 compared to the observations. This difference is more (less) negative for more absorbing (reflecting) dust, in particular over India. Since this region is also influenced by sulfate and carbonaceous aerosols, the simulated optical thickness is not inconsistent with the observation.

The atmospheric dust load in the model is evidently overestimated offshore western Australia during SH summer. During the other seasons, in particular during SH spring, the emissions from this region seem to be more realistic. The simulated optical thickness is only slightly higher than the one from the satellite retrievals.

There are evidently negative differences between the simulated optical thickness and the AVHRR data in regions where the effect of soil dust aerosols is small, for

example, central America during the NH spring. These differences are caused by maxima of the optical thickness in the AVHRR satellite retrievals. Those maxima can be attributed to sulfate and carbonaceous aerosols, which are not taken into consideration in our study.

6.3. Comparison of Interannual Variability

To evaluate the model capability to reproduce the interannual variability of the dust load in the atmosphere, we also compared the standard deviation of the seasonally averaged values. In regions with high dust optical thickness such as in the Arabian Sea, the model tends to overestimate the standard deviation compared to the observations, especially if the mean optical thickness is also overestimated. In contrast, in regions with low optical thickness, the simulated variability is evidently lower than the observed one. In the latter case, this could be explained by the neglecting of other aerosol types, which have a strong influence in those regions where the dust aerosol optical thickness is low.

7. Globally Averaged Climate Response

For all seasons the global mean of certain climate variables in the passive dust experiment, and their changes in the experiments with radiatively active dust are presented in Table 6. Regional variations will be described in a future article.

In the baseline experiment, the perturbation of net radiation due to radiative forcing by dust is about $-0.4\,\mathrm{W\,m^{-2}}$ at TOA and $-1.7\,\mathrm{W\,m^{-2}}$ at surface; that is, the main effect of soil dust aerosols is to redistribute radiative heating from the surface to the atmospheric column. This well agrees with the results obtained by *Miller and Tegen* [1998]. Compared to those, however, the response is less negative at surface and corresponds to greater cooling at TOA. *Miller and Tegen* [1998] studied the climate response using a prescribed distribution of the dust concentration and the nine layer version of the GISS AGCM coupled to a mixed layer ocean model. Thus the difference in the response could represent differences in the model, especially in the treatment of the ocean, or it may represent a measure of the uncertainty of model estimates of dust radiative forcing.

Both at TOA and surface, a negative anomaly by solar radiation is counteracted by a smaller positive anomaly by thermal radiation. In the annual average in both spectral ranges, the effect at surface is about 4 times the effect at TOA. The difference between top and surface anomaly is largest during NH summer and smallest during winter. The perturbation of absorbed solar radiation has an evident annual cycle with a minimum of $0.9\,\mathrm{W\,m^{-2}}$ in autumn and a maximum of $2.0\,\mathrm{W\,m^{-2}}$ in summer. This corresponds to different dust concentrations in the atmosphere in these two seasons (see Table 3).

Higher absorptivity of the dust particles additionally decreases the net radiative flux at surface and increases the radiative gain at TOA compared to the baseline experiment. Higher reflectivity has a reversed effect. The globally averaged solar radiation at surface is very sensitive to the particle single-scattering albedo, in particular during NH summer. This is related to a strong sensitivity of the absorbed solar radiation in the atmospheric column; the absorbed solar radiation due to the radiative dust effect is in the case of more absorbing dust roughly twice the value of the baseline experiment and 12 times the value of the experiment with more reflecting dust. The emitted thermal radiation at the surface decreases with increased absorptivity due to larger cooling at surface under the dust cloud. In contrast, the anomaly of backscattered solar radiation at TOA decreases with increased absorptivity (i.e., decreased reflectivity) of the dust particles.

Even during NH winter, when the dust concentration is most reduced for more absorbing dust compared to the other experiments with radiatively active dust (see Table 3), the anomaly of absorbed solar radiation is largest in this experiment. In addition, during NH summer the negative anomaly of solar radiation at TOA is largest in the experiment for more reflecting dust, indicating a stronger backscattering effect, although the dust concentration is most reduced here; that is, the direct effect of the changed radiative forcing due to variations in the single-scattering albedo of dust particles (maybe combined with an effect due to changes in total cloud cover) dominates the effect of the changed optical thickness due to the sensitivity of the atmospheric dust concentration to the single-scattering albedo of dust particles.

Other variables are also sensitive to the radiative properties of dust particles. The globally averaged sensible heat flux at surface, which is negative, becomes significantly less negative with higher absorptivity to balance the reduced surface net radiation. The surface net heating shows a negative response to the radiative effect of dust. The decrease, which is larger for more reflecting than for more absorbing dust, indicates that the radiative effect of dust tries to cool the surface. However, the lower boundary condition was prescribed in our experiments so that the SST cannot adapt to the surface net heat flux. For this reason the global aver-

aged surface air temperature is not listed in Table 6.

Both precipitation and evaporation decrease in the experiments, which include the radiative effect of dust, in particular for more absorbing dust. The total cloud cover shows a slight tendency of increase (decrease) for more absorbing (reflecting) dust, except in NH summer. In this season the cloud cover diminishes in all experiments that include the radiative effect of dust.

8. Summary and Conclusions

Four experiments with a soil dust model embedded in the NASA GISS AGCM were carried out. In one of them, dust was a passive tracer whose radiative effect was omitted. In the others, dust radiative forcing was allowed to influence the model climate. The size- and wavelength-dependent single-scattering albedo of far-traveled Saharan dust was prescribed for dust from all source regions in one of those experiments. However, dust optical properties should vary with the mineralogical content of the source region. In order to estimate the importance of this effect, without undertaking the computational burden of parameterizing each source region individually, we repeated the experiment with radiatively active dust, this time increasing or decreasing by 10% the single-scattering albedo of the dust particles for all source regions and wavelengths.

The implementation of the radiative effect of dust into the model generally led to a reduced soil dust cycle on a global scale compared to the experiment where dust is transported as dynamic but radiatively inactive tracer; that is, there is a negative feedback in the climate system due to the radiative effect of dust which counteracts the emission of soil dust. The reduction varies with the radiative properties of dust. During NH winter the strongest decrease is found for more absorbing dust, and during summer, the strongest decrease is found for more reflecting dust.

The detailed analysis of the emission in the various main dust source regions showed that the reduction varies both with the season and with the radiative properties of dust particles. In NH winter, lowering (raising) the single-scattering albedo by 10% led to reduced (increased) dust emission in the Sahara/Sahel source region, compared to the baseline experiment. In contrast, in NH summer, the reduction is smallest (largest) for more absorbing (reflecting) dust in this region. In summer, such a sensitivity was also found for the Arabian Peninsula source region and the region around the Aral Sea. In both regions, even an increase in the emission was found for more absorbing dust, compared to the experiment with radiatively inactive dust. In contrast, in all seasons the dust emission in the east Asia source region is reduced to a greater (lesser) extent for more absorbing (reflecting) dust compared to the baseline experiment. A similar dependence on the single-scattering albedo was found for the North America source region, in particular for its southern part. For the Australia source region, in SH summer there is not any clear dependence of the emission on the radiative effect of dust particles.

We studied the relation of the changes in dust emission to changes in the surface wind for each season using correlation coefficients calculated from monthly averaged values. For the Sahara/Sahel source region, and the Arabian Peninsula, we found an evidently positive correlation between dust emission and large-scale circulation features represented by the magnitude of the monthly averaged surface wind vector. During NH winter in our experiments, the dust emission and its change with varying radiative properties of dust is related to the trade winds over the Sahara/Sahel area. In summer, a relation to the Indian monsoon circulation was found in the eastern Sahara and the Arabian Peninsula. The increase (decrease) in the dust emission from the Arabian Peninsula for more absorbing (reflecting) dust is connected to an increased (decreased) monsoon circulation. In the case of other dust source regions we did not find a relation of the emission to large-scale circulation patterns but to the mean surface wind speed that is based on daily values. This indicates that processes with short timescales mainly determine the changes in the dust source flux in most source regions.

We did not find any significant correlation between changes in the difference of precipitation and evaporation and changes in the dust source flux. However, the modeled evaporation is highly constrained and so therefore is the precipitation, because the SST was prescribed in our experiments. In addition, soil moisture, and therefore the evaporation, changes with a characteristic time of a few months. Calculating the instantaneous correlation, instead of taking a time lag into account, may not be the most appropriate approach. Hence the possible role of a feedback between the difference of precipitation and evaporation and the radiative effect of dust on decadal timescales remains largely unknown due to the limitations of the current study. These feedbacks will be reexamined in future studies using the GISS AGCM coupled to a mixed layer and a dynamic ocean model.

The changes in the mean dust concentration as well as in the dust removal both due to the implementa-

tion of the radiative effect of dust and their sensitivity to single-scattering albedo are consistent with the results from the analysis of the dust emission. For all seasons, we also compared the standard deviations of the seasonally averaged dust concentration in the various experiments to examine the interannual variability in the model. During all seasons, the variability decreases in the regions with maximum dust concentration in all experiments with radiatively active dust compared to the experiment with inactive dust, if the long-term mean of the concentration also decreases. In NH summer the variability increases over the Arabian Peninsula and central Asia, if the radiative effect of dust is implemented, in particular for more absorbing dust and in the baseline experiment.

To evaluate the model capability to reproduce the average dust concentration and the interannual variability in all seasons, we compared the optical thickness simulated in the experiments to the observations from AVHRR satellite data. The simulated optical thickness agrees well with the observed one in NH winter over the North Atlantic, indicating a reliable dust concentration in the model in this region. Results, which are not inconsistent with the observations, were also obtained for the ocean regions east of east Asia during NH spring and over India during spring and summer. In contrast, the model seems to overestimate the dust optical thickness over North Africa during spring, over the Arabian Peninsula, and central Asia during summer, and over Australia during SH summer. Presumably, where the model simulations are poor, the source mechanism does not faithfully capture the complex interaction of wind speed, vegetation, soil moisture, and soil features that determine erosion. In these regions where the verisimilitude of model-predicted dust burden is low, the sensitivity of the source mechanism to radiative feedbacks is unknown because the source mechanism itself is not adequately represented in the model. In regions, such as North Africa during winter, where the model credibly predicts at least the large-scale patterns of erosion, we can have much greater confidence in the results of the sensitivity study. However, since the satellite retrievals used for this comparison are based on a single-channel algorithm and therefore necessarily assume aerosol properties (some of which are more appropriate for sulfate than dust aerosols), this comparison is somewhat ambiguous.

The model tends to overestimate the interannual variability in regions with high dust optical thickness compared to satellite data, in particular if the mean optical thickness is also overestimated. In contrast, in regions with low optical thickness the simulated variability is evidently lower than the observed one. The latter result might be related to an underestimated transport of fine particles by the model to regions far from the sources but is probably due to the fact that the satellite retrieval is determined by other aerosol types in those regions with low dust concentration.

In the baseline experiment, the dust aerosols from all source regions had the radiative properties of far-traveled Saharan dust particles. However, the conclusion from our sensitivity experiments is that specifying the radiative properties appropriate for individual source regions might improve the simulated dust emission because of the different sensitivity of the soil dust emission to changing radiative features of dust. For this, variations in the mineralogical composition of dust need to be taken into account [*Sokolik and Toon*, 1999; *Claquin et al.*, 1999].

Corresponding to the sensitivity of the soil dust cycle, we also found a sensitivity of various climate variables, such as TOA and surface radiation, temperature, precipitation, cloud cover, and circulation to the radiative properties of dust particles. The sensitivity of the globally averaged climate variables we showed here is dominated by the direct effect due to the radiative properties of the dust particles (maybe combined with an effect due to changes in total cloud cover), which generally overwhelms the effect of the changed optical thickness due to the sensitivity of the atmospheric dust concentration to the dust radiative forcing. The sensitivity of the climate response will be described in more detail in a companion paper. The effect on trade winds in North Africa and Indian monsoon circulation has already been a part of the analysis presented here.

Given the negative feedback by dust radiative forcing on dust emission, it has to be explained why, in the source regions of North Africa and the Arabian Peninsula, the strongest decrease in the dust emission in winter is found for more absorbing dust particles but in summer for more reflecting dust particles. We suggest two competing mechanisms are responsible for this behavior in our experiments. Absorption of solar radiation in the dust layer leads to a redistribution of energy from the surface into the dust layer. Hence the temperature increases in the dust layer, having a locally stabilizing effect on the atmosphere. This effect causes a decrease in the surface wind speed on shorter timescales leading to the general decrease in the dust emission; that is, there is a negative feedback. This feedback is larger for more absorbing than for more reflecting dust particles, as shown for the globally averaged solar radiation in

section 7. Therefore in general the amount of emitted dust should decrease the most in the experiments with more absorbing dust particles. During summer, in the source regions of North Africa and the Arabian Peninsula, the local radiative effect is overwhelmed by the changes in the wind speed on longer timescales, caused by an increased (decreased) Indian monsoon circulation for more absorbing (reflecting) dust shown in section 3, leading to the reversed sensitivity during this season. Since these source regions contribute the most to the global dust load, this behavior of the sensitivity is also seen for the globally integrated dust emissions. However, the reliability of the link between the radiative properties of soil dust aerosols and the Indian monsoon found in our experiments and the physical mechanism behind this link remain open questions at this time which have to be addressed in future studies.

Since the experiments described in this paper are the first experiments with a soil dust aerosol model which is fully coupled in a AGCM, we do not know at this time how robust our results are. Our experiments were carried out with a prescribed SST. The next step will be to repeat these experiments using the NASA GISS AGCM coupled to a mixed layer ocean. In this way, we want to examine whether the results are robust, if the SST itself is calculated and the energy fluxes depending on it are included in the system of feedbacks. In order to assess the magnitude of the full feedback between dust cycle and climate response, it will be desirable to repeat such model experiments with the atmospheric GCM coupled to a dynamic ocean.

Acknowledgments. We thank two anonymous reviewers for helpful suggestions. This work was supported by grant ATM-97-27872 of the Climate Dynamics Program of the National Science Foundation.

References

Alpert, P., Y. J. Kaufman, Y. Shay-El, D. Tanre, A. da Silva, S. Schubert, and J. H. Joseph, Quantification of dust-forced heating of the lower troposphere, *Nature*, *395*, 367–370, 1998.

Claquin, T., M. Schulz, Y. Balkanski, and O. Boucher, Uncertainties in assessing radiative forcing by mineral dust, *Tellus*, *Ser. B, 50*, 491–505, 1998.

Claquin, T., M. Schulz, and Y. J. Balkanski, Modeling the mineralogy of atmospheric dust sources, *J. Geophys. Res.*, *104*, 22,243–22,256, 1999.

Coakley, J. A., and R. D. Cess, Response of the NCAR Community Climate Model to the radiative forcing by the naturally occurring tropospheric aerosol, *J. Atmos. Sci.*, *42*, 1677–1692, 1985.

Del Genio, A. D., and M. S. Yao, Efficient cumulus parameterization for long-term climate studies: The GISS scheme, *Am. Meteorol. Soc. Monogr.*, *46*, 181–184, 1993.

Del Genio, A. D., M.-S. Yao, W. Kovari, and K. K.-W. Lo, A prognostic parameterization for global climate models, *J. Clim.*, *9*, 270–304, 1996.

Dentener, F. J., G. R. Carmichael, Y. Zhang, J. Lelieveld, and P. J. Crutzen, Role of mineral aerosol as a reactive surface in the global troposphere, *J. Geophys. Res.*, *101*, 22,869–22,889, 1996.

Druyan, L. M., K. P. Shah, K.-W. K. Lo, J. A. Marengo, and G. Russell, Impacts of model improvements on general circulation model sensitivity to sea-surface temperature forcing, *Int. J. Climatol.*, *15*, 1061–1086, 1995.

Duce, R. A., Sources, distribution, and fluxes of mineral aerosol and their relationship to climate, in *Aerosol Forcing of Climate*, edited by R. J. Charlson, and J. Heintzenberg, vol. ES17, pp. 43–72, John Wiley, New York, 1995.

Genthon, C., Simulations of desert dust and sea salt aerosols in Antarctica with a general-circulation model of the atmosphere, *Tellus*, *Ser. B, 44*, 371–389, 1992.

Gillette, D., A wind tunnel simulation of the erosion of soil: Effect of soil texture, sandblasting, wind speed, and soil consolidation on dust production, *Atmos. Environ.*, *12*, 1735–1743, 1978.

Hansen, J., et al., Forcing and chaos in interannual to decadal climate change, *J. Geophys. Res.*, *102*, 25,679–25,720, 1997.

Hansen, J. E., G. L. Russell, D. Rind, P. Stone, A. Lacis, S. Lebedeff, R. Ruedy, and L. Travis, Efficient three-dimensional global models for climate studies: Model I and II, *Mon. Weather Rev.*, *111*, 609–662, 1983.

Hartke, G. J., and D. Rind, Improved surface and boundary layer models for the Goddard Institute for Space Studies general circulation model, *J. Geophys. Res.*, *102*, 16,407–16,422, 1997.

Herman, J. R., P. K. Bhartia, O. Torres, C. Hsu, C. Seftor, and E. Celarier, Global distribution of UV-absorbing aerosols from Nimbus-7/TOMS data, *J. Geophys. Res.*, *102*, 16,911–16,922, 1997.

Husar, R. B., J. M. Prospero, and L. L. Stowe, Characterization of tropospheric aerosols over the oceans with the NOAA advanced very high resolution radiometer optical thickness operational product, *J. Geophys. Res.*, *102*, 16,889–16,909, 1997.

Joussaume, S., Three-dimensional simulations of the atmospheric cycle of desert dust particles using a general circulation model, *J. Geophys. Res.*, *95*, 1909–1941, 1990.

Lacis, A. A., and M. I. Mishchenko, Climate forcing, climate sensitivity, and climate response: A radiative modeling perspective on atmospheric aerosols, in *Aerosol Forcing of Climate*, edited by R. J. Charlson, and J. Heintzenberg, pp. 11–42, John Wiley, New York, 1995.

Li, X., H. Maring, D. Savoie, K. Voss, and J. M. Prospero, Dominance of mineral dust in aerosol light-scattering in the North Atlantic trade winds, *Nature*, *380*, 416–419,

1996.

Liao, H., and J. H. Seinfeld, Radiative forcing by mineral dust aerosols: Sensitivity to key variables, *J. Geophys. Res.*, *103*, 31,637–31,645, 1998.

Liousse, C., J. E. Penner, C. Chuang, J. J. Walton, and H. Eddleman, A global three-dimensional model study of carbonaceous aerosols, *J. Geophys. Res.*, *101*, 19,411–19,432, 1996.

Marticorena, B., and G. Bergametti, Two-year simulations of seasonal and interannual changes of the Saharan dust emissions, *Geophys. Res. Lett.*, *23*, 1921–1924, 1996.

Matthews, E., Global vegetation and land use: New high-resolution databases for climate studies, *J. Clim. Appl. Meteorol.*, *22*, 474–487, 1983.

Middleton, N. J., and D. S. G. Thomas, *World Atlas of Desertification*, Edward Arnold, London, 1992.

Miller, R. L., and I. Tegen, Climate response to soil dust aerosols, *J. Clim.*, *11*, 3247–3267, 1998.

Miller, R. L., and I. Tegen, Radiative forcing of a tropical direct circulation by soil dust aerosols, *J. Atmos. Sci.*, *56*, 2403–2433, 1999.

Moulin, C., C. E. Lambert, F. Dulac, and U. Dayan, Control of atmospheric export of dust from North Africa by the North Atlantic Oscillation, *Nature*, *387*, 691–693, 1997.

Patterson, E. M., and D. A. Gillette, Commonalities in measured size distributions for aerosols having a soil-derived component, *J. Geophys. Res.*, *82*, 2074–2082, 1977.

Penner, J. E., C. C. Chuang, and K. Grant, Climate forcing by carbonaceous and sulfate aerosols, *Clim. Dyn.*, *14*, 839–851, 1998.

Prospero, J., The atmospheric transport of particles to the ocean, in *Particle Flux in the Ocean*, edited by V. Ittekkot et al., pp. 19–26, John Wiley, New York, 1996.

Rao, C. R. N., L. L. Stowe, E. P. McClain, J. Sapper, and M. P. McCormick, Development and application of aerosol remote sensing with AVHRR data from the NOAA satellites, in *Aerosol and Climate*, edited by P. V. Hobbs, A. Deepak, Hampton, Va., 1988.

Rind, D., and J. Lerner, Use of on-line tracers as a diagnostic tool in general circulation model development, 1, Horizontal and vertical transport in the troposphere, *J. Geophys. Res.*, *101*, 12,667–12,683, 1996.

Rosenzweig, C., and F. Abramopoulos, Land-surface model development for the GISS GCM, *J. Clim.*, *10*, 2040–2054, 1997.

Schulz, M., Y. J. Balkanski, W. Guelle, and F. Dulac, Role of aerosol size distribution and source location in a three-dimensional simulation of a Saharan dust episode tested against satellite-derived optickal thickness, *J. Geophys. Res.*, *103*, 10,579–10,592, 1998.

Shine, K. P., and P. M. de F. Forster, The effect of human activity on radiative forcing of climate change: A review of recent developments, *Global Planet Change*, *20*, 205–225, 1999.

Sokolik, I. N., and O. B. Toon, Incorporation of mineralogical composition into models of the radiative properties of mineral aerosol from UV to IR wavelengths, *J. Geophys. Res.*, *104*, 9432–9444, 1999.

Stowe, L. L., A. M. Ignatov, and R. Singh, Development, validation, and potential enhancements to the second-generation operational aerosol product at the National Environmental Satellite, Data, and Information Service of the National Oceanic and Atmospheric Administration, *J. Geophys. Res.*, *102*, 16,923–16,934, 1997.

Tabazadeh, A., M. Z. Jacobson, H. B. Singh, O. B. Toon, J. S. Lin, R. B. Chatfield, A. N. Thakur, R. W. Talbot, and J. E. Dibb, Nitric acid scavenging by mineral and biomass burning aerosol, *Geophys. Res. Lett.*, *25*, 4185–4188, 1998.

Tegen, I., and I. Fung, Modeling of mineral dust in the atmosphere: Sources, transport, and optical thickness, *J. Geophys. Res.*, *99*, 22,897–22,914, 1994.

Tegen, I., and I. Fung, Contribution to the atmospheric mineral aerosol load from land surface modification, *J. Geophys. Res.*, *100*, 18,707–18,726, 1995.

Tegen, I., and A. A. Lacis, Modeling of particle influence on the radiative properties of mineral dust aerosol, *J. Geophys. Res.*, *101*, 19,237–19,244, 1996.

Tegen, I., and R. Miller, A general circulation model study on the interannual variability of soil dust aerosol, *J. Geophys. Res.*, *103*, 25,975–25,995, 1998.

Tegen, I., A. A. Lacis, and I. Fung, The influence on climate forcing of mineral aerosols from disturbed soils, *Nature*, *380*, 419–422, 1996.

Tegen, I., P. Hollrigl, M. Chin, I. Fung, D. Jacob, and J. Penner, Contribution of different aerosol species to the global aerosol extinction optical thickness, *J. Geophys. Res.*, *102*, 23,895–23,915, 1997.

Tegen, I., D. Koch, A. A. Lacis, and M. Sato, Trends in tropospheric aerosol loads and corresponding impact on direct radiative forcing between 1950 and 1990: A model study, *J. Geophys. Res.*, *105*, 26,071–26,989, 2000.

Tucker, C. J., H. E. Dregne, and W. W. Newcomb, Expansion and contraction of the Sahara desert from 1980 to 1990, *Science*, *253*, 299–301, 1991.

Volz, F. E., Infrared optical constants of ammonium sulfate, Sahara dust, volcanic pumice, and flyash, *Appl. Opt.*, *12*, 564–568, 1973.

Webb, R., C. Rosenzweig, and E. R. Levine, A global data set of particle size properties, *Tech. Rep. TM-4286*, 33 pp., NASA, 1991.

World Resources Institute (WRI), *World Resources 1992-1993*, edited by A. L. Hammond, Oxford Univ. Press, New York, 1992.

Zobler, L., A world soil file for global climate modeling, *Tech. Rep. TM-87802*, 32 pp., NASA, 1986.

R. L. Miller, NASA Goddard Institute for Space Studies, 2880 Broadway, New York, NY 10025. (rmiller@giss.nasa.gov)

J. Perlwitz, Department of Applied Physics and Applied Mathematics, Columbia University, c/o NASA GISS, 2880 Broadway, New York, NY 10025. (jperl-

witz@giss.nasa.gov)

I. Tegen, Max Planck Institute for Biogeochemistry, Tatzendpromenade 1a, D-07745 Jena, Germany. (itegen@bgc-jena.mpg.de)

Received February 11, 2000; revised July 21, 2000; accepted October 5, 2000.

[1]Also at NASA Goddard Institute for Space Studies, New York.

This preprint was prepared with AGU's LaTeX macros v5.01.
File dust1˙4p formatted May 2, 2001.

Table 1. Seasonal and Annual Global Amounts of Emitted Dust in $\mathrm{Mt\,month^{-1}}$ and $\mathrm{Mt\,yr^{-1}}$ in the Passive Dust Experiment (P) and in Experiments With Radiatively Active Dust for More Absorbing Dust ($0.9\varpi_0$), Baseline Dust (ϖ_0), and More Reflecting Dust ($1.1\varpi_0$)

	P		$0.9\varpi_0$		ϖ_0		$1.1\varpi_0$	
Season	Mean	STDV	Mean	STDV	Mean	STDV	Mean	STDV
DJF	114	17	90	14	100	14	100	11
MAM	128	15	100	11	106	16	107	14
JJA	119	21	114	13	107	19	93	12
SON	76	14	57	8	61	12	59	10
ANN	1312	97	1081	71	1120	88	1073	68

Long-term means and standard deviations (STDV) are presented.

Table 2. Seasonal and Annual Amounts of Emitted Dust in Mt month^{-1} and Mt yr^{-1} From Source Regions in the Passive Dust Experiment (P) and in Experiments With Radiatively Active Dust for More Absorbing Dust ($0.9\varpi_0$), Baseline Dust (ϖ_0), and More Reflecting Dust ($1.1\varpi_0$)

	P		$0.9\varpi_0$		ϖ_0		$1.1\varpi_0$	
Season	Mean	STDV	Mean	STDV	Mean	STDV	Mean	STDV
			Sahara/Sahel Dust Emission					
DJF	62	12	48	12	55	10	59	10
MAM	65	12	53	8	55	11	56	10
JJA	51	13	52	10	46	10	42	8
SON	19	5	15	5	16	5	16	5
ANN	592	55	501	53	517	54	519	42
			Arabian Peninsula Dust Emission					
DJF	6.7	2.3	6.0	2.3	6.4	2.1	6.5	2.0
MAM	3.0	1.9	2.1	1.1	2.2	0.9	2.1	1.0
JJA	7.1	2.9	10.7	5.3	7.4	2.7	4.4	1.5
SON	2.1	1.2	2.0	1.0	1.7	0.8	2.2	1.3
ANN	56.5	11.9	62.4	17.4	53.2	11.8	45.7	9.4
			Central Asia Dust Emission					
DJF	1.8	1.2	1.3	0.9	2.1	1.7	1.9	1.7
MAM	20.6	10.4	16.0	8.1	15.6	8.8	14.5	5.9
JJA	35.7	13.5	33.5	12.5	30.9	18.3	22.9	7.3
SON	12.5	8.2	7.8	7.7	8.2	6.2	7.2	3.9
ANN	211.0	58.4	174.8	55.5	169.4	63.2	138.8	25.2
			East Asia Dust Emission					
DJF	0.6	0.6	0.5	0.4	0.7	0.9	0.5	0.5
MAM	13.1	5.8	9.6	4.0	10.1	4.0	11.5	4.6
JJA	3.8	2.1	1.4	1.5	2.6	1.7	3.1	1.7
SON	1.0	1.0	0.5	0.8	1.0	0.8	1.0	1.0
ANN	55.2	21.5	35.9	12.3	42.6	13.5	47.8	14.4
			North America Dust Emission					
DJF	7.9	3.8	5.7	2.2	6.6	3.2	5.0	2.1
MAM	14.7	7.1	10.2	4.5	12.6	5.3	11.7	5.3
JJA	7.4	4.2	4.2	3.1	5.8	3.0	5.9	3.0
SON	8.4	5.0	5.2	2.9	8.6	4.8	6.1	2.7
ANN	114.8	41.7	75.7	21.3	100.5	25.0	86.3	24.6
			Australia Dust Emission					
DJF	33.4	11.3	27.2	6.0	27.8	7.1	25.6	5.6
MAM	9.1	4.4	6.9	2.1	7.7	2.6	7.9	2.5
JJA	7.2	2.5	5.4	2.0	6.1	2.9	6.3	2.9
SON	25.1	9.0	19.8	5.7	18.2	6.6	18.3	6.2
ANN	225.2	53.7	178.6	28.2	179.7	35.9	175.0	24.8

Long-term means and standard deviations (STDV) are presented.

Table 3. Globally Averaged Dust Concentration $\mu g\,kg^{-1}$(Air) Averaged Over All Layers in the Passive Dust Experiment (P) and in Experiments With Radiatively Active Dust for More Absorbing Dust ($0.9\varpi_0$), Baseline Dust (ϖ_0), and More Reflecting Dust ($1.1\varpi_0$)

	P		$0.9\varpi_0$		ϖ_0		$1.1\varpi_0$	
Season	Mean	STDV	Mean	STDV	Mean	STDV	Mean	STDV
DJF	3.46	0.51	2.83	0.42	2.99	0.36	3.00	0.36
MAM	4.54	0.54	3.65	0.35	3.79	0.54	3.70	0.50
JJA	4.32	0.68	4.21	0.56	3.81	0.67	3.29	0.38
SON	2.53	0.47	2.28	0.27	2.02	0.27	1.81	0.27
ANN	3.71	0.25	3.24	0.22	3.15	0.26	2.95	0.19

Long-term means and standard deviations (STDV) are presented.

Table 4. Seasonal and Annual Global Amounts of Wet Deposition of Dust in $Mt\,month^{-1}$ and $Mt\,yr^{-1}$ in the Passive Dust Experiment (P) and in Experiments With Radiatively Active Dust for More Absorbing Dust ($0.9\varpi_0$), Baseline Dust (ϖ_0), and More Reflecting Dust ($1.1\varpi_0$)

	P		$0.9\varpi_0$		ϖ_0		$1.1\varpi_0$	
Season	Mean	STDV	Mean	STDV	Mean	STDV	Mean	STDV
DJF	46	7	34	5	38	5	37	5
MAM	53	7	39	5	42	6	42	5
JJA	59	10	55	6	51	7	45	6
SON	35	6	25	4	27	4	25	3
ANN	579	42	461	27	472	32	449	26

Long-term means and standard deviations (STDV) are presented.

Table 5. Seasonal and Annual Global Amounts of Dry Turbulent Deposition of Dust in $\mathrm{Mt\,month^{-1}}$ and $\mathrm{Mt\,yr^{-1}}$ in the Passive Dust Experiment (P) and in Experiments With Radiatively Active Dust for More Absorbing Dust ($0.9\varpi_0$), Baseline Dust (ϖ_0), and More Reflecting Dust ($1.1\varpi_0$)

	P		$0.9\varpi_0$		ϖ_0		$1.1\varpi_0$	
Season	Mean	STDV	Mean	STDV	Mean	STDV	Mean	STDV
DJF	16.7	2.3	14.2	2.6	15.7	2.3	16.1	2.0
MAM	19.5	2.8	15.7	1.8	16.7	2.9	17.2	2.8
JJA	16.6	2.9	16.4	2.5	16.2	4.0	14.1	1.7
SON	11.7	2.4	9.0	1.8	9.5	1.9	9.2	1.7
ANN	193.8	14.4	166.2	13.5	175.1	16.9	170.1	12.1

Long-term means and standard deviations (STDV) are presented.

Table 6. Global Mean of Various Climate Variables (Long-Term Mean Plus or Minus One Standard Deviation) in the Passive Dust Experiment (P) and Their Perturbations in Experiments With Radiatively Active Dust for More Absorbing Dust ($0.9\varpi_0$), Baseline Dust (ϖ_0), and More Reflecting Dust ($1.1\varpi_0$)

Season	P	$0.9\varpi_0$	ϖ_0	$1.1\varpi_0$
	TOA Net Radiation ($W\,m^{-2}$)			
DJF	9.0 ± 0.4	-0.2	-0.5	-0.7
MAM	0.5 ± 0.4	0.2	-0.3	-0.8
JJA	-8.6 ± 0.4	-0.3	-0.5	-0.5
SON	3.4 ± 0.3	-0.2	-0.4	-0.5
ANN	1.1 ± 0.2	-0.1	-0.4	-0.6
	TOA Solar Radiation ($W\,m^{-2}$)			
DJF	238.3 ± 0.4	-0.3	-0.6	-0.8
MAM	230.6 ± 0.4	0.3	-0.3	-0.8
JJA	224.4 ± 0.3	-0.0	-0.5	-0.7
SON	234.7 ± 0.4	-0.4	-0.6	-0.7
ANN	232.0 ± 0.1	-0.1	-0.5	-0.7
	TOA Thermal Radiation ($W\,m^{-2}$)			
DJF	-229.3 ± 0.2	0.1	0.1	0.1
MAM	-230.1 ± 0.2	-0.0	0.1	$+0.0$
JJA	-233.0 ± 0.2	-0.3	$+0.0$	0.2
SON	-231.3 ± 0.2	0.2	0.2	0.2
ANN	-231.0 ± 0.1	-0.0	0.1	0.1
	Surface Net Radiation ($W\,m^{-2}$)			
DJF	119.6 ± 0.2	-2.3	-1.7	-1.0
MAM	112.2 ± 0.2	-2.6	-1.9	-1.3
JJA	107.5 ± 0.2	-3.3	-2.0	-1.0
SON	116.6 ± 0.2	-1.9	-1.1	-0.7
ANN	114.0 ± 0.1	-2.5	-1.7	-1.0
	Surface Solar Radiation ($W\,m^{-2}$)			
DJF	170.7 ± 0.4	-3.2	-2.0	-1.0
MAM	164.3 ± 0.4	-3.8	-2.2	-1.1
JJA	158.3 ± 0.4	-5.0	-2.5	-1.0
SON	168.0 ± 0.4	-2.9	-1.5	-0.8
ANN	165.3 ± 0.2	-3.7	-2.1	-1.0
	Surface Thermal Radiation ($W\,m^{-2}$)			
DJF	-51.1 ± 0.3	0.9	0.3	$+0.0$
MAM	-52.1 ± 0.3	1.2	0.4	-0.2
JJA	-50.9 ± 0.2	1.7	0.5	-0.1
SON	-51.5 ± 0.2	1.0	0.4	0.1
ANN	-51.4 ± 0.1	1.2	0.4	-0.0
	Surface Sensible Heat Flux ($W\,m^{-2}$)			
DJF	-23.0 ± 0.2	1.1	0.7	0.2
MAM	-26.0 ± 0.2	1.6	0.8	0.1
JJA	-27.1 ± 0.2	1.9	0.9	0.1
SON	-23.7 ± 0.2	0.9	0.4	0.1
ANN	-25.0 ± 0.1	1.4	0.7	0.2

Table 6. (continued)

Season	P	$0.9\varpi_0$	ϖ_0	$1.1\varpi_0$
	Surface Net Heating ($W\,m^{-2}$)			
DJF	8.2 ± 0.5	-0.2	-0.4	-0.6
MAM	-2.1 ± 0.4	-0.1	-0.5	-0.7
JJA	-9.5 ± 0.4	-0.2	-0.4	-0.6
SON	4.8 ± 0.5	0.2	-0.3	-0.5
ANN	0.4 ± 0.2	-0.1	-0.4	-0.6
	Precipitation ($mm\,d^{-1}$)			
DJF	3.01 ± 0.02	-0.03	-0.02	-0.00
MAM	3.00 ± 0.02	-0.04	-0.02	-0.01
JJA	3.07 ± 0.01	-0.04	-0.02	-0.01
SON	3.03 ± 0.01	-0.04	-0.01	-0.00
ANN	3.03 ± 0.01	-0.04	-0.02	-0.01
	Evaporation ($mm\,d^{-1}$)			
DJF	3.02 ± 0.02	-0.03	-0.02	-0.00
MAM	3.01 ± 0.02	-0.03	-0.02	-0.01
JJA	3.07 ± 0.02	-0.04	-0.02	-0.01
SON	3.00 ± 0.01	-0.04	-0.01	-0.00
ANN	3.03 ± 0.01	-0.04	-0.02	-0.01
	Total Cloud Cover (%)			
DJF	51.4 ± 0.2	0.2	-0.1	-0.1
MAM	50.2 ± 0.2	0.1	-0.1	-0.3
JJA	51.4 ± 0.2	-0.2	-0.0	-0.1
SON	51.1 ± 0.2	0.4	0.2	$+0.0$
ANN	51.0 ± 0.1	0.2	-0.0	-0.1

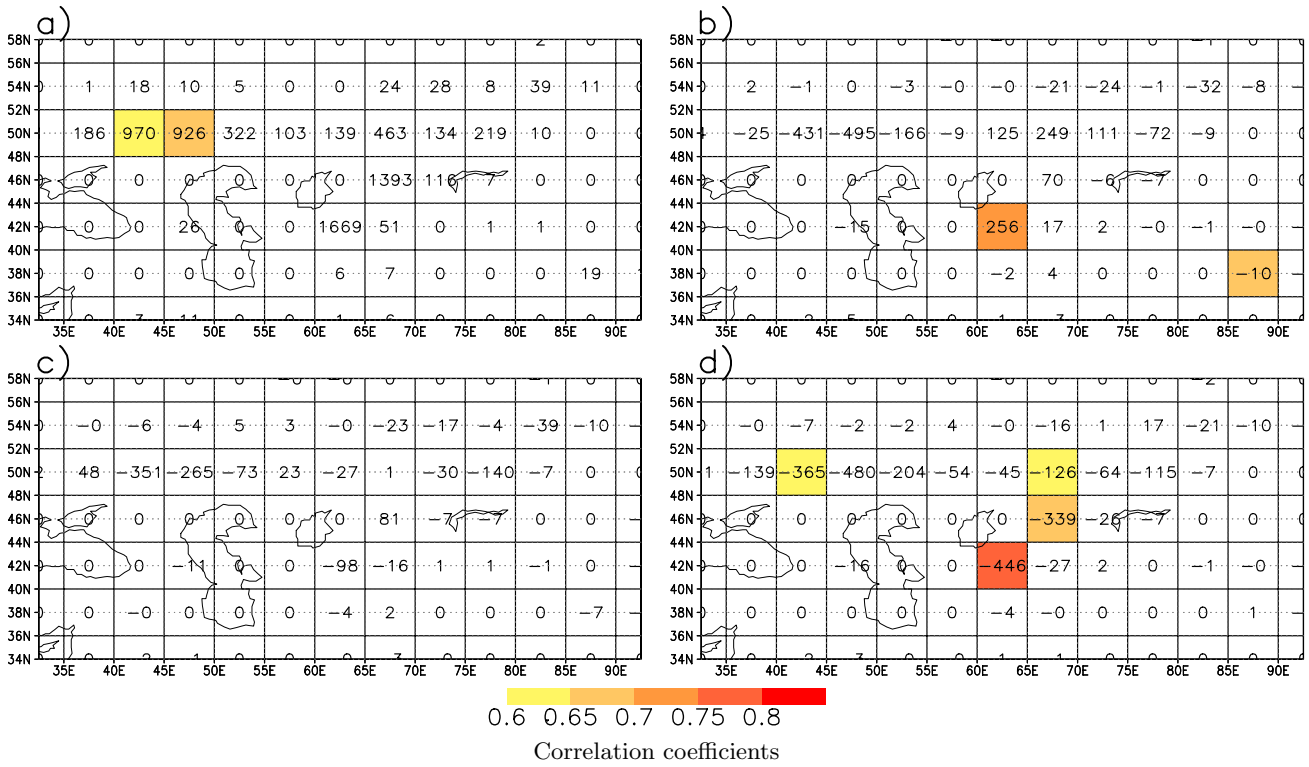

Figure 1. Dust source flux (numbers) ($\mathrm{mg\,m^{-2}\,d^{-1}}$) and correlation (shades) between dust source flux and surface wind speed in the central Asia source region in NH summer. (a) Passive dust experiment; difference to passive dust experiment for (b) more absorbing dust, (c) baseline experiment, and (d) more reflecting dust.

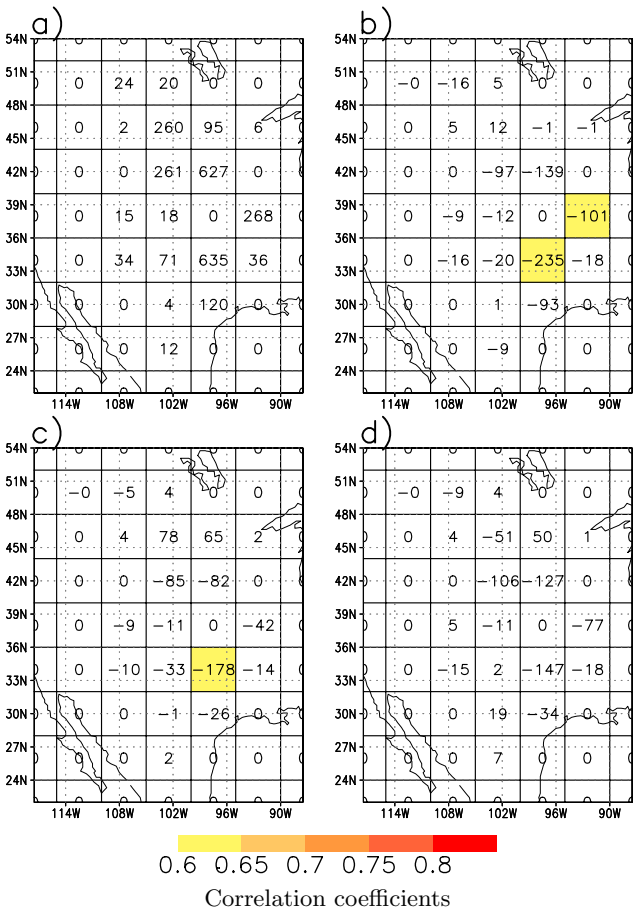

Figure 2. Dust source flux (numbers) ($\mathrm{mg\,m^{-2}\,d^{-1}}$), and correlation (shades) between dust source flux and surface wind speed in the North America source region in NH spring. (a) Passive dust experiment; difference to passive dust experiment for (b) more absorbing dust, (c) baseline experiment, and (d) more reflecting dust.

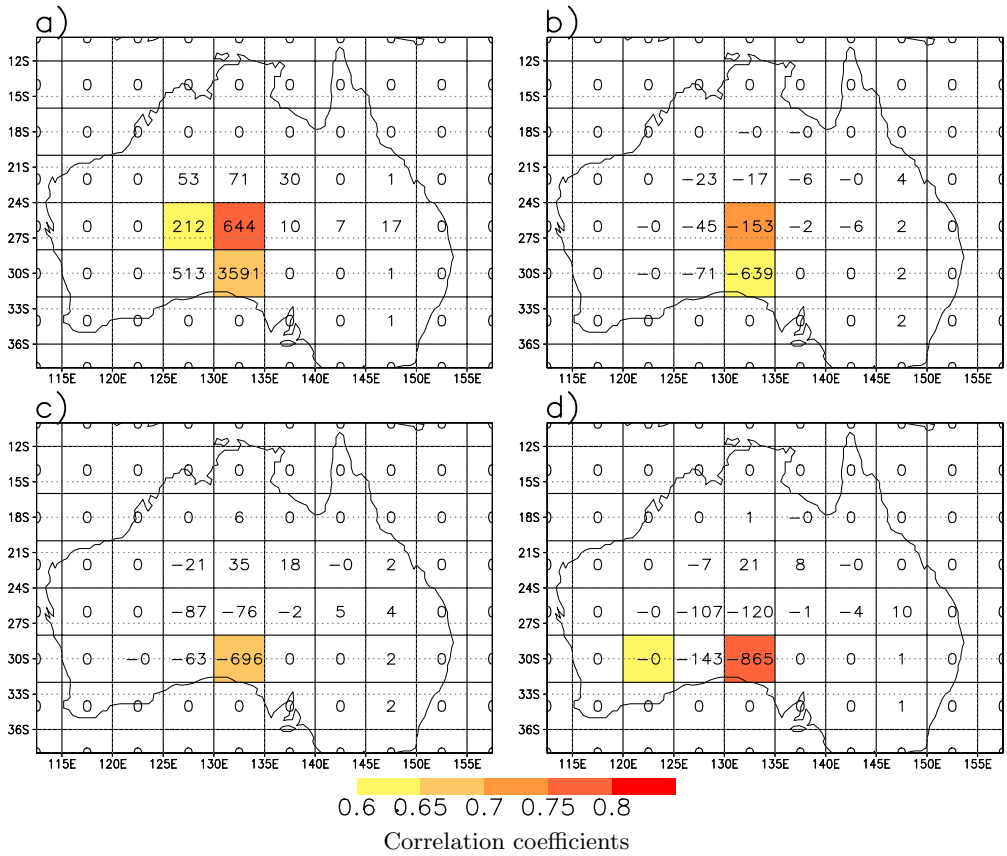

Figure 3. Dust source flux (numbers) ($\mathrm{mg\,m^{-2}\,d^{-1}}$), and correlation (shades) between dust source flux and surface wind speed in the Australia source region in Southern Hemisphere (SH) summer. (a) Passive dust experiment; difference to passive dust experiment for (b) more absorbing dust, (c) baseline, and (d) more reflecting dust.

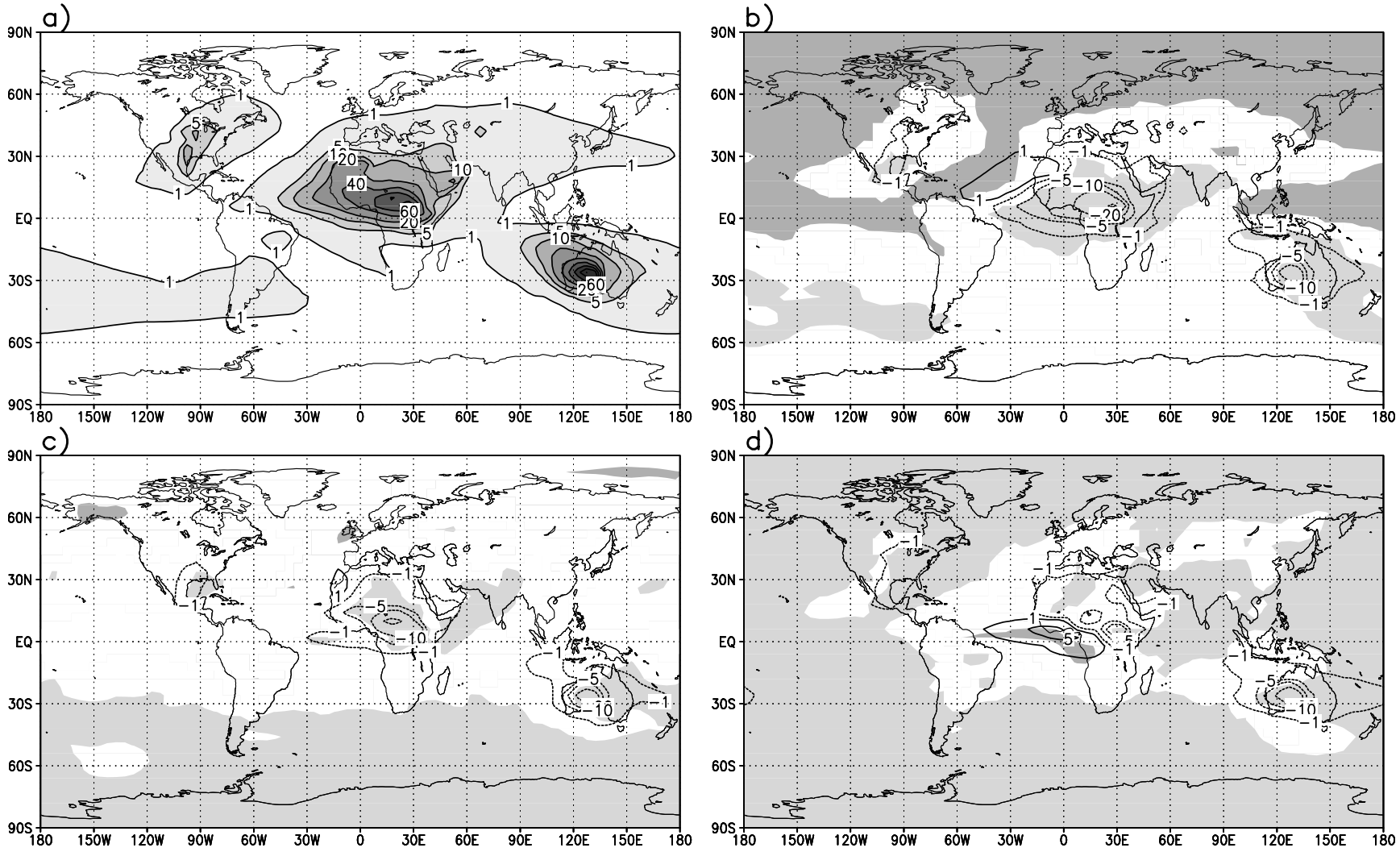

Figure 4. Dust concentration ($\mu g\,kg^{-1}$) averaged over all layers in NH winter: (a) passive dust experiment; difference to passive dust experiment for (b) more absorbing dust, (c) baseline experiment, and (d) more reflecting dust. The light (dark) shades in Figure 4b, 4c, and 4d indicate statistically significant decreases (increases) at a confidence level of 95% or greater.

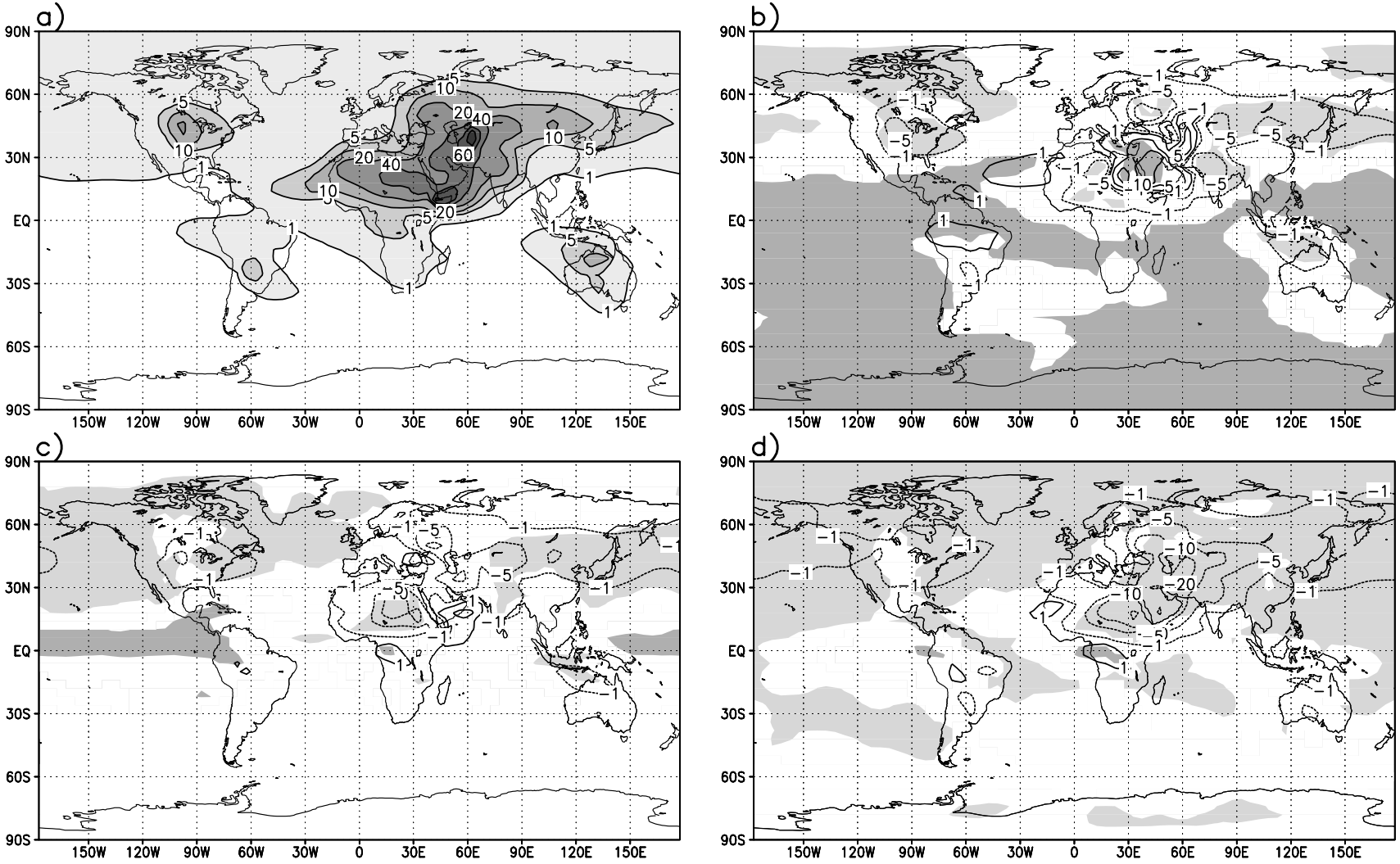

Figure 5. Same as in Figure 4 but in NH summer.

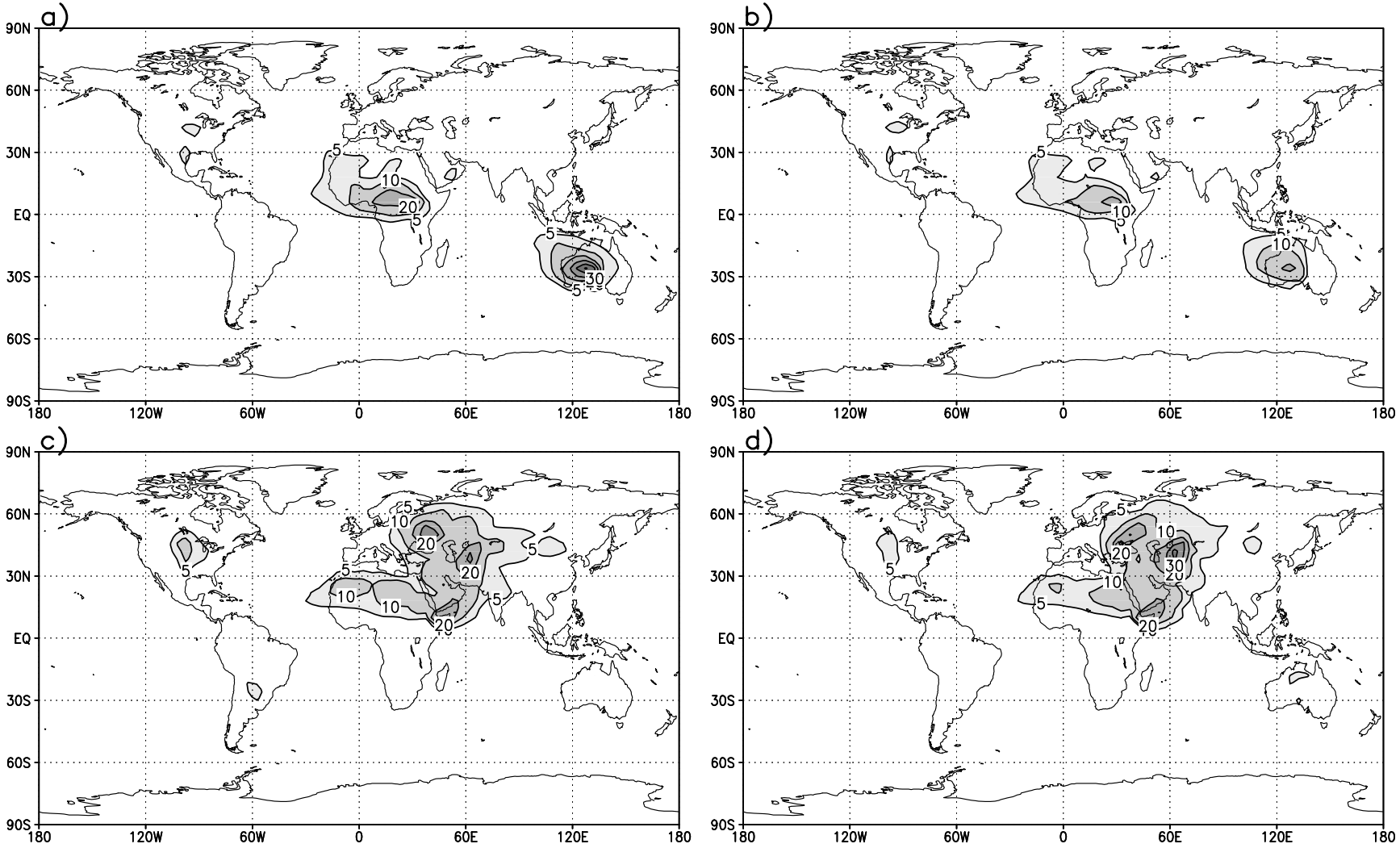

Figure 6. Seasonal standard deviation of the dust concentration ($\mu g\,kg^{-1}$): (a) passive dust experiment and (b) baseline experiment in NH winter; (c, d) same as Figure 6a and 6b but in summer.

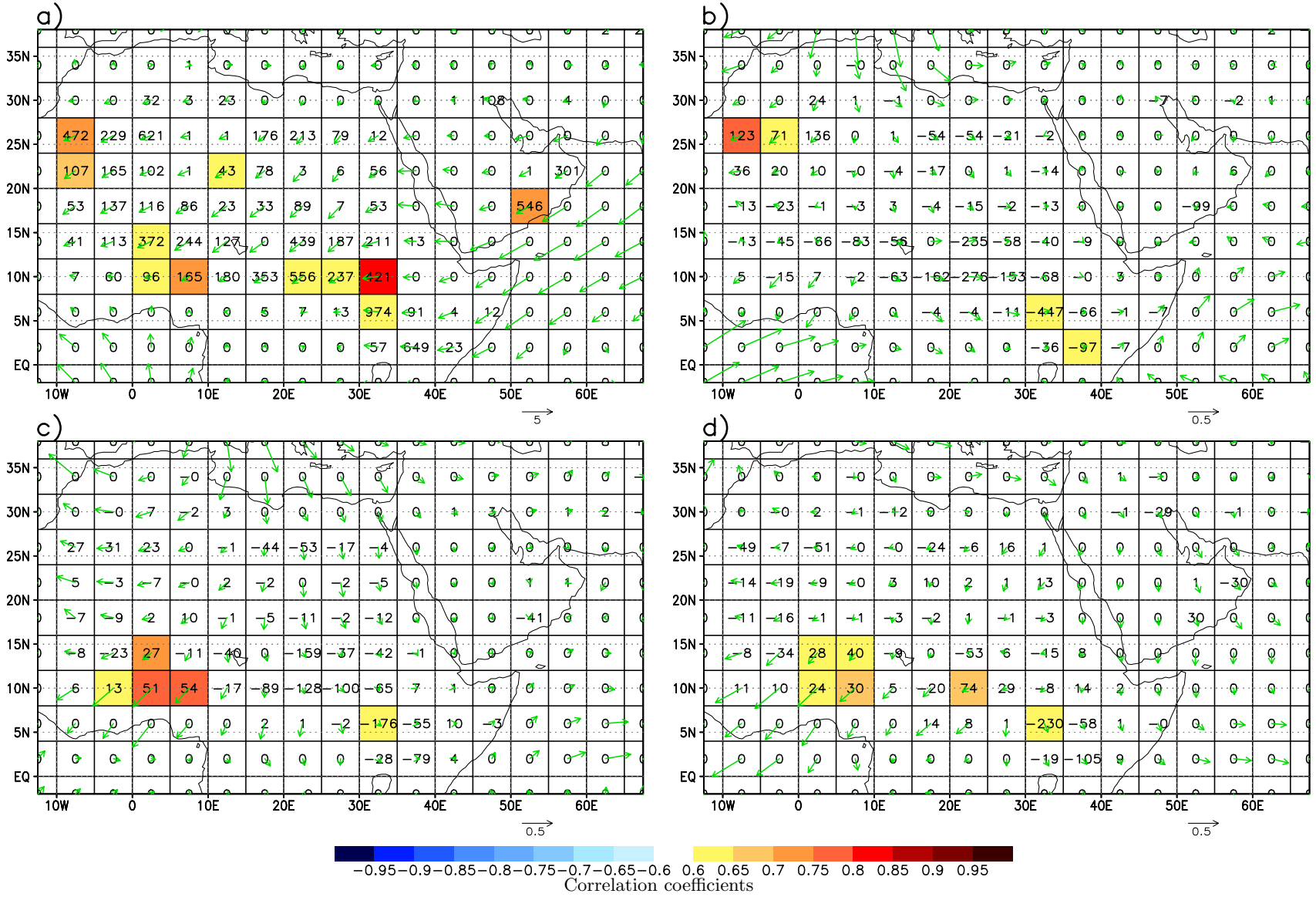

Plate 1. Dust source flux (numbers) ($\mathrm{mg\,m^{-2}\,d^{-1}}$), surface wind vector (arrows) ($\mathrm{m\,s^{-1}}$), and correlation (shades) between dust source flux and magnitude of the monthly averaged surface wind vector in the Sahara/Sahel source region and in the Arabian Peninsula source region in Northern Hemisphere (NH) winter. (a) Passive dust experiment; difference to passive dust experiment for (b) more absorbing dust, (c) baseline experiment, and (d) more reflecting dust.

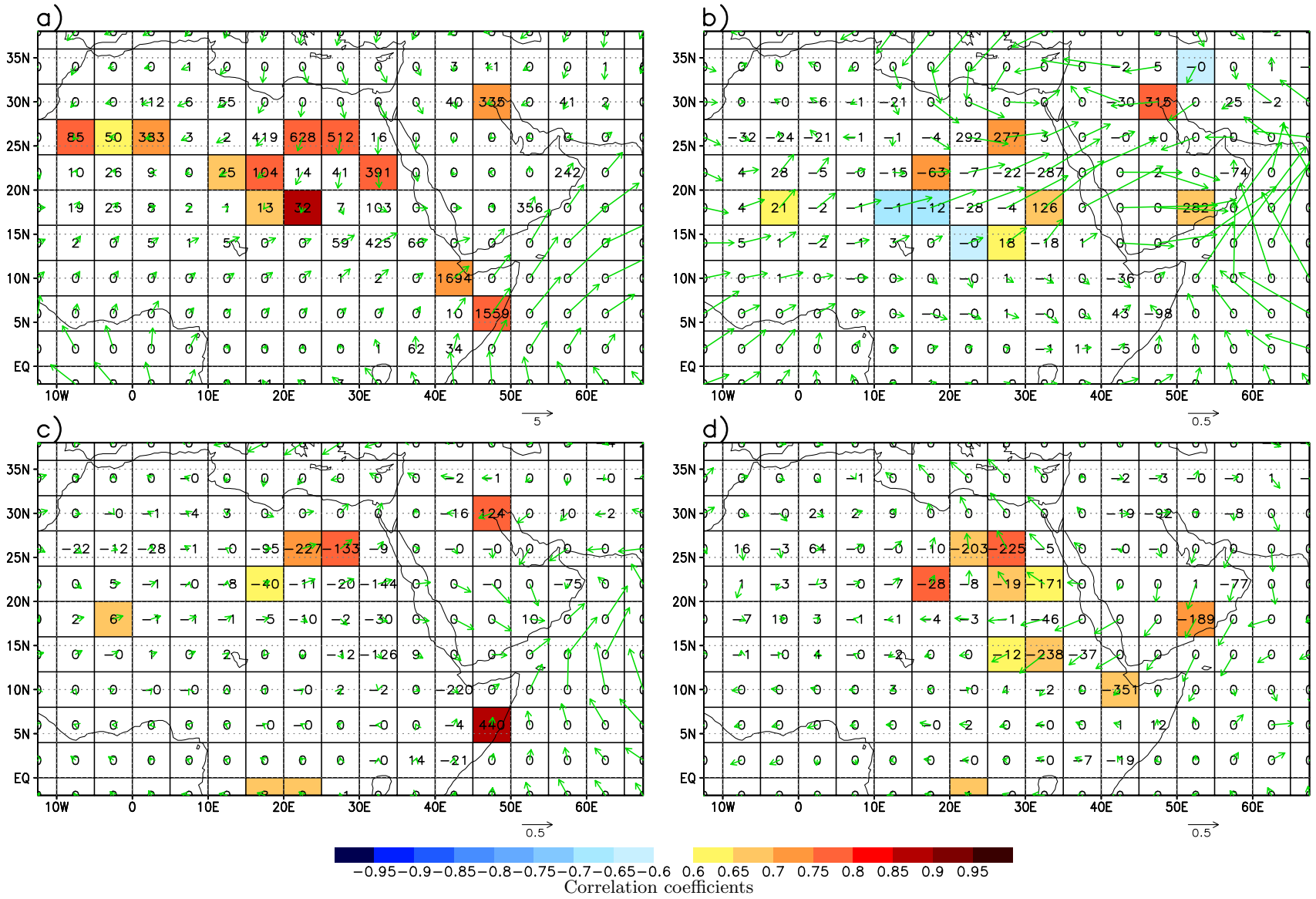

Plate 2. Same as Plate. 1 but in NH summer.

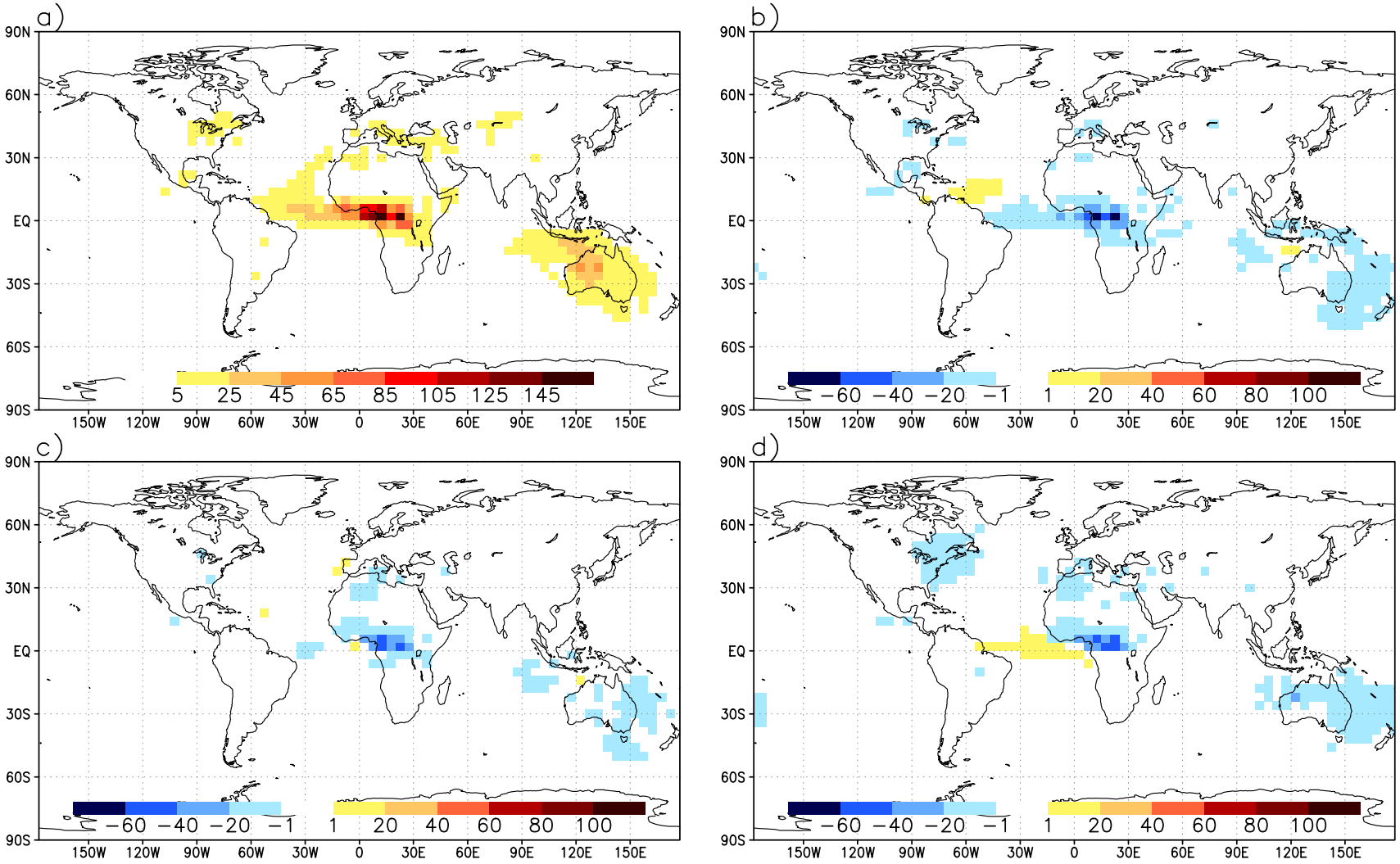

Plate 3. Wet deposition of dust ($\mathrm{mg\,m^{-2}\,d^{-1}}$) in NH winter. (a) Passive dust experiment; statistically significant differences to passive dust experiment for (b) more absorbing dust, (c) baseline experiment, and (d) more reflecting dust.

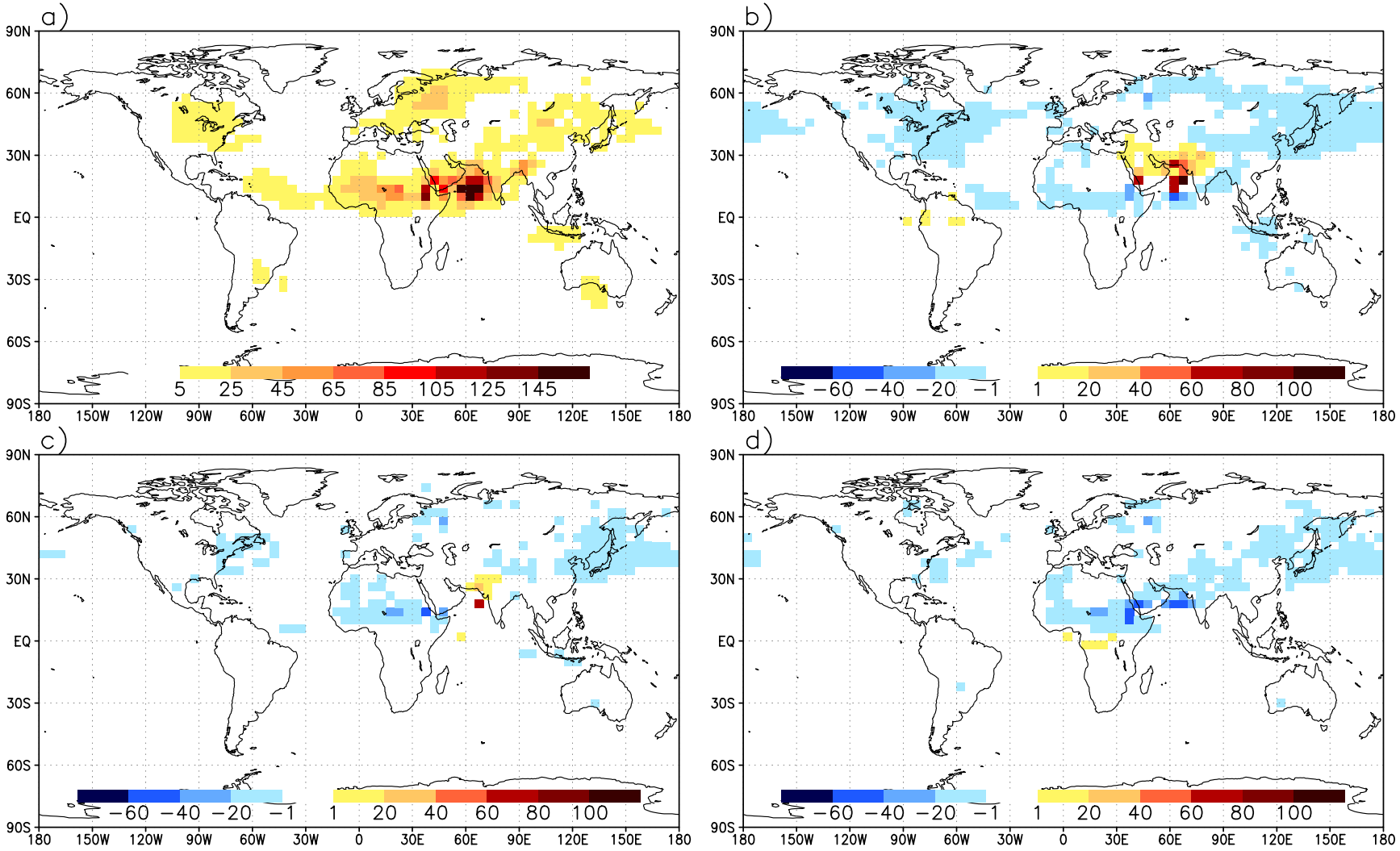

Plate 4. Same as in Plate 3 but in NH summer.

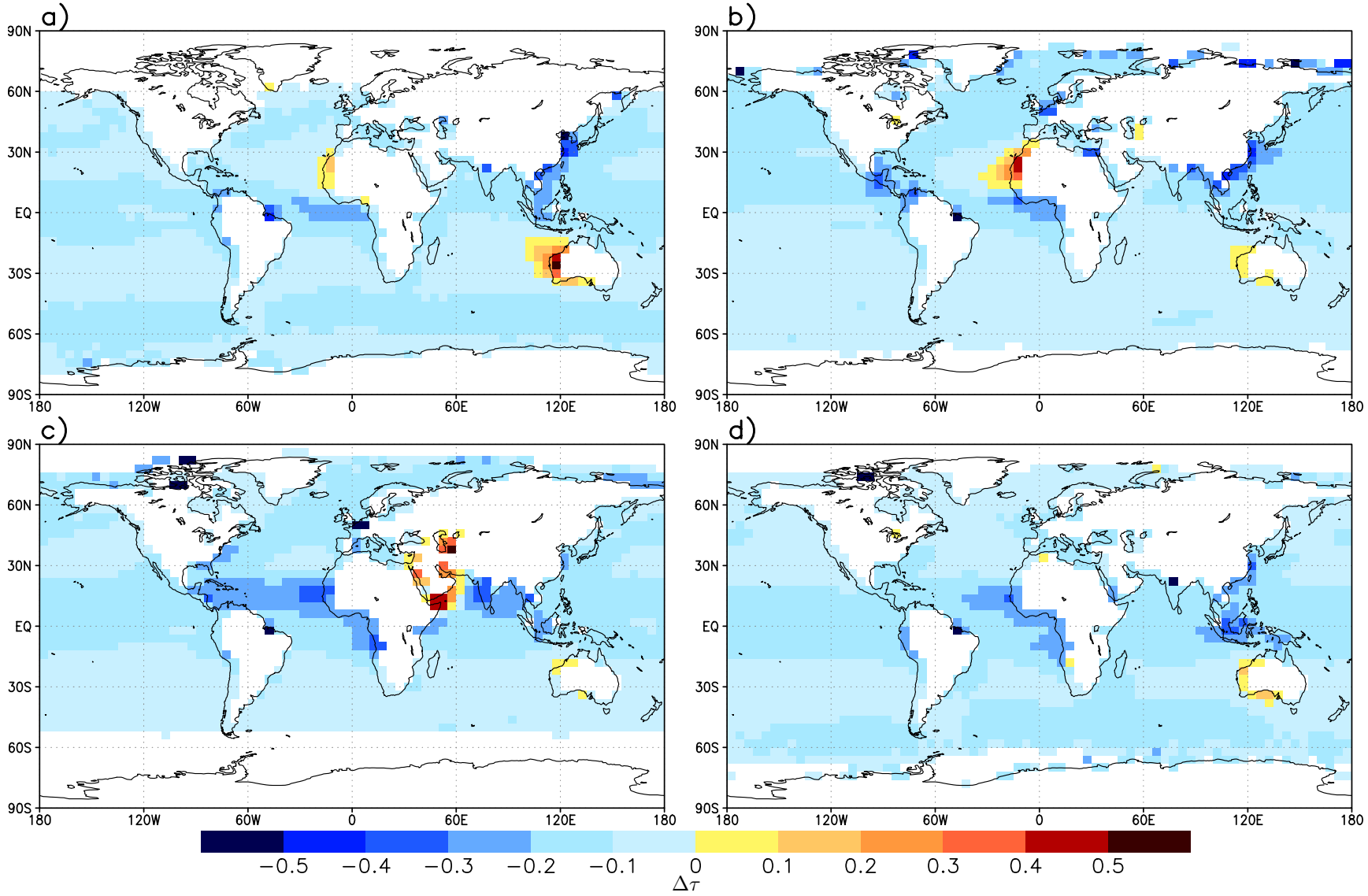

Plate 5. Difference between dust optical thickness (τ) in the baseline experiment and AVHRR satellite data for (a) NH winter, (b) spring, (c) summer, and (d) autumn.